Mon. Not. R. astr. Soc. (1990) **246**, 576–596

Photometry of distant clusters of galaxies: evolutionary features in the cluster 2158 + 0351 ($z = 0.45$)

Emilio Molinari,[1] Alberto Buzzoni[2] and Guido Chincarini[1,2]

[1] *Università degli Studi di Milano, Via Celoria, 16, 20133 Milano, Italy*
[2] *Osservatorio Astronomico di Brera, Via Brera, 28, 20121 Milano, Italy*

Accepted 1990 April 20. Received 1990 April 18; in original form 1989 July 14

SUMMARY

Results of detailed three-colour photometry of the distant cluster 2158 + 0351 ($z = 0.445$) are presented. A photometric catalogue has been produced using the INVENTORY package, for which we give an estimate of completeness and photometric errors. In total we measured Gunn *g*, *r*, *i* magnitudes for 294 objects, down to $r = 23.5$, with a typical error of 0.1 mag. On the basis of a statistical analysis, about 60 per cent of these are suggested to be cluster members. Luminosity functions are shown along with colour–magnitude and two-colour diagrams. We find that the bright-cluster galaxy population is dominated by ellipticals, while a population of spirals becomes relevant at the faint luminosities. Such an overabundance of faint spirals leads us to calculate a high fraction of blue objects, according to the Butcher–Oemler effect. We find $f_B = 0.30 \pm 0.13$. We evidence possible photometric effects on magnitudes and colours due to galactic evolution. In particular, elliptical galaxies in the cluster are recognized to be bluer than present-day descendants, and the first-ranked galaxy is intrinsically brighter by about 0.8 mag. An independent estimate of the redshift of the cluster, through photometric properties of its galaxy population, is attempted, deriving $z = 0.44 \pm 0.05$. This is obtained taking into account appropriate evolutionary *k*-corrections from population-synthesis models. The importance of such a correction when studying high redshift (young) galaxies is stressed.

1 INTRODUCTION

Progress in observational cosmology crucially depends on the detection of objects at large distances. Of course, the definition of 'large distance' is somewhat relative and arbitrary, depending on the particular problem we are dealing with. The deduced look-back time could be compared with the collapse time of a system, with stellar evolutionary ages or, referring to the determination of cosmological parameters, with the value of z at which different world models become observationally distinguishable.

Clusters of galaxies play a fundamental role in this sense. They can be detected at high redshifts ($z \sim 1$), and some of their present properties can be fairly well investigated and understood. Due to the presence of intergalactic hot gas, clusters of galaxies are powerful X-ray sources (for a recent review, see Chincarini 1989), and therefore can be used as tracers of the distribution of matter in the Universe. In well selected samples, they also give clues about the motion on large scale (Peebles 1980; Bahcall 1988; Scaramella *et al.* 1989).

Overall photometric properties of galaxies in distant clusters stem directly from the evolutionary status of their stellar populations. A better knowledge of this relationship would certainly lead to a more confident use of galaxy populations in approaching other phenomena relevant to cluster evolution in the early stages of the Universe (Gunn & Dressler 1988).

The purpose of this paper is to outline our procedure for the study of galaxy population in the cluster 2158 + 0351 at $z = 0.445$ (Gunn, Hoessel & Oke 1986). The present work further updates and refines the preliminary results previously presented (Buzzoni *et al.* 1988; Molinari 1988).

We describe observations and image-processing procedures in Sections 2 and 3, where details on the photometric calibration are also given. The photometric catalogue obtained and the related astrophysical parameters are presented in Section 4, and discussed in Section 5. Comparison with the expectations stemming from the models for evolutionary stellar-population synthesis is performed in Section 6, where we also attempt to estimate photometrically the value of z. Section 7 summarizes the results obtained.

2 OBSERVATIONS AND REDUCTIONS

Three observing nights, in 1986 November, were allotted at the ESO 3.6-m telescope at La Silla (Chile). Observations were performed with the EFOSC focal reducer at the Cassegrain focus. The detector was an RCA 640 × 1032 CCD (ESO no. 8), in the binned operating model. Original pixels of 15 × 15 μm^2 size were rebinned to give an effective size of 30 μm and a scale of 0.675 arcsec pixel^{-1}. The field retained for our analysis is a rectangle of 3.2 × 5.3 arcmin^2 corresponding to an absolute dimension of 1.45 × 2.41 (50/H_0) Mpc at the cluster.

Fair, although not excellent, seeing conditions provided a 1.3–1.4 arcsec FWHM point-spread function throughout the observing run. Table 1 lists the journal of observations. All the frames of the standard stars were taken by defocusing the telescope, owing to their relative brightness (around the eleventh magnitude).

Observations were performed in the Gunn *g*, *r*, *i* photometric system (Thuan & Gunn 1976; Wade *et al.* 1979). Effective wavelengths and passband widths are reported in Table 2, while the instrumental response is given in Fig. 1.

Table 1. Journal of observations.

Date	Field	Filter	Exp Time (sec)
1986 Nov 5	Cluster	g	1500
	Cluster	r	1500
	Cluster	i	1500
	FEIGE 11	r	10
	FEIGE 11	i	20
	FEIGE 16	g	10
	FEIGE 16	g	10
	FEIGE 16	r	10
	FEIGE 16	i	20
	L - 284	g	10
	L - 284	g	5
	L - 284	r	3
	L - 284	i	6
	L - 284	i	3
	L - 249	g	5
	L - 249	g	5
	L - 249	r	5
	L - 249	i	5
	L - 351	g	5
	L - 351	g	5
	L - 351	r	5
	L - 351	i	5
	L - 346	g	5
	L - 346	r	3
	L - 346	r	3
	L - 346	i	3
1986 Nov 7	Cluster	r	1200
	Cluster	i	600
	Cluster	g	600
	Cluster	r	300

Table 2. Response of the photometric system.

Filter	λ_{eff}(Å) (this work)	$\Delta\lambda$(Å) (this work)	λ_{eff}(Å) (Thuan & Gunn, 1976)	$\Delta\lambda$(Å) (Thuan & Gunn, 1976)
g	5100	800	4930	700
r	6800	1100	6500	900
i	7900	1300	8200* (7900)**	1300* (1300)**

* Wade *et al.* 1979
** Schneider *et al.* 1983

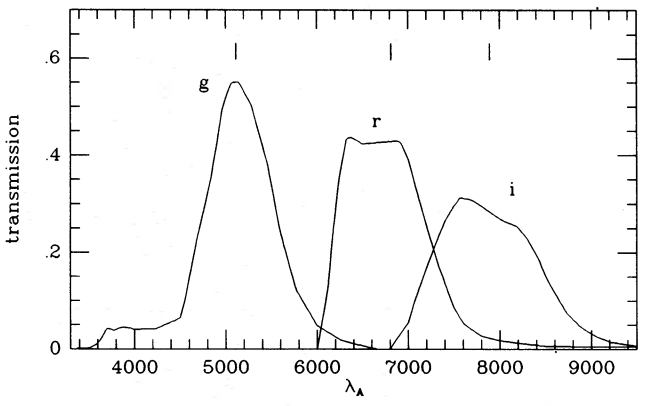

Figure 1. Response curves for the photometric system used in this work. The absolute transparency of ESO-Gunn filter + CCD #8 + EFOSC camera is plotted. Effective wavelengths are marked on the top.

Here we show the convolution of ESO, *g*, *r*, *i* Gunn filters with CCD and EFOSC responses, as obtained from the ESO-EFOSC Operating Manual (Dekker & D'Odorico 1985).

Two different sets of flat-field frames were taken in each filter, using twilight and dome-diffused sunlight. All frame manipulation was performed using the MIDAS system elaborated by ESO and installed at the Osservatorio Astronomico of Brera, Milano (see MIDAS Users Guide, Image Processing Group, ESO V4.3, 1988).

We found a major problem in frame reduction, since the EFOSC camera suffered severe contamination by scattered light. As a result, a rather bright circular ghost image appeared in the centre of all frames, affecting the background by about 7 per cent. A preliminary cleaning procedure was necessary to allow the confident detection and measurement of faint objects in the cluster. Thus a model for the scattered light was constructed, and its smoothed pattern subtracted from every image (cluster and flat frames) after proper scaling. In order to increase the signal-to-noise level, single frames of the cluster were re-coordinated by forcing a grid of bright stars to collimate in the different frames and these were then added together. Total exposure time was 35 min for *g* and *i*, and 50 min for *r*. More than 10^6 photons were collected for the brightest galaxies in the cluster. As a result of the coadding procedure, the point-spread function degraded to about 2 arcsec FWHM in the different bands. A direct evaluation of our reduction procedure can be done using Fig. 2, where three pictures of the cluster (in *g*, *r* and *i*, respectively) are displayed. Fringing in the *i*-band was not fully removed, and some features still appear in the final frame. However, as we discuss in Subsection 3.3, this has not caused serious problems with object photometry.

3 DATA ANALYSIS

Recognition and measurement of (possibly) all the objects present in the frames is a first preliminary requirement to be met for our subsequent analysis. Therefore, we need (i) a reliable automatic detection algorithm assuring completeness at a given magnitude level, and (ii) accurate multicolour photometry providing magnitudes and colours for all of the objects detected.

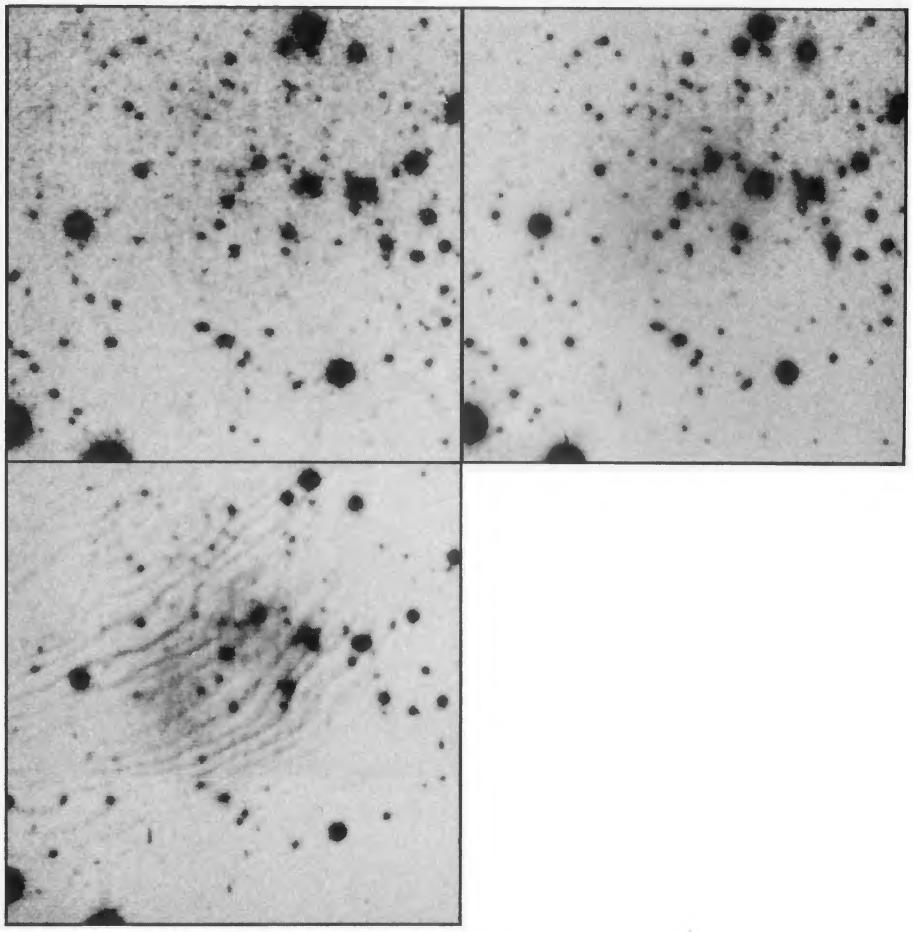

Figure 2. A picture of the field around the cluster 2158 + 0351. Each panel is a co-added image of two or three original frames. Top left is the *g* frame, top right the *r* frame and bottom left the *i* frame. The total equivalent exposure time is 30 min for *g* and *i*, and 50 min for *r* (3.6-m ESO telescope + EFOSC). North is up and east to the right.

The whole procedure should work homogeneously in the different bands of observation; in fact it is clear that the size of our database is constrained by the non-detections in the worst frame.

3.1 Completeness and galaxy discrimination

Systematic detection in the different co-added frames was performed by means of the INVENTORY package (West & Kruszewski 1981) implemented on MIDAS. This package allows detailed study of the astronomical images, and also attempts to classify the extended (galaxies), stellar and spurious features, through the study of their shape and apparent surface brightness. Magnitudes can be obtained for each object, both over fixed circular apertures and at a given isophotal level.

For our specific aims, we preferred using the algorithm only in its detection mode, searching for all objects rising by more than 1 per cent over local background, and overriding automatic classification. As shown in Fig. 3, galaxies at high redshift are expected to appear as essentially unsampled features on the CCD frames, since they are only a few pixels across. Furthermore, their brightness profiles are strongly seeing-limited, and no relevant deviations from the point-spread function are expected.

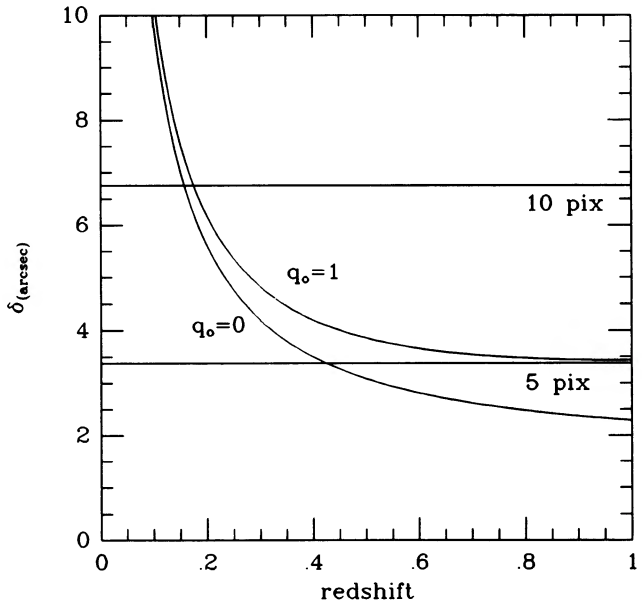

Figure 3. Angular dimension of a 25-kpc diameter galaxy at various redshifts for $H_0 = 50$ km s^{-1} Mpc^{-1} and two values for the cosmological parameter q_0. The two horizontal lines show the size of 5 and 10 pixels on our frames.

Direct tests performed with INVENTORY revealed that the automatic classification procedure fails in firmly discriminating between galaxies and stars fainter than 21st magnitude. The threshold of discrimination depends crucially on the size of the extended objects. Further checks on clusters at lower redshift ($z \sim 0.2$), for example, reveal that in this case galaxies are still recognized at $r \simeq 23$. Fig. 4 shows the characteristic bifurcation obtained in the distribution of the isophotal radii of the detected objects in the r frame plotted versus their magnitude. It can be clearly seen that bright galaxies have apparent radii systematically larger than stars at the same magnitude, while faint galaxies merge with stars. This method of discrimination is basically equivalent to other photometric and morphological indices adopted by other authors, e.g. the multi-ring photometry by Kron (1980), Koo *et al.* (1986) and Iannicola *et al.* (1987).

As a general conclusion, we believe that a deterministic discrimination of very distant galaxies on the basis of their apparent morphological features could prove to be impossible (unless one has available excellent images at subarcsec seeing), and severe biases could possibly be introduced in the study of cluster-galaxy populations. In our opinion, an alternative approach relying on the colour properties of the galaxies (Ellingson *et al.* 1989; Rakos, Fiala & Schombert 1988) would be much better. As we will discuss in more detail in Section 4.1, such an approach has proved to be the most fruitful and effective for our study.

In order to evaluate the completeness achieved by INVENTORY in detecting low-signal-to-noise features, we have performed a number of tests using original frames to produce new artificial images with known intrinsic properties. Typically, the procedure involved a single frame which was axially reversed and rotated to produce three supplementary images. They were then progressively merged to generate three new frames with a 2-, 3- and 4-fold enhanced object density with respect to the original frame. Application of the detection algorithm to the sequence of images (after proper normalization to the background) provided the total number of detections to be compared with those expected by simply scaling for density increase. This allowed us to test detection efficiency at the different isophotal levels, also providing a quantitative evaluation of crowding losses. The results are summarized in Fig. 5, where the relative detection efficiency is displayed versus the true mean object density.

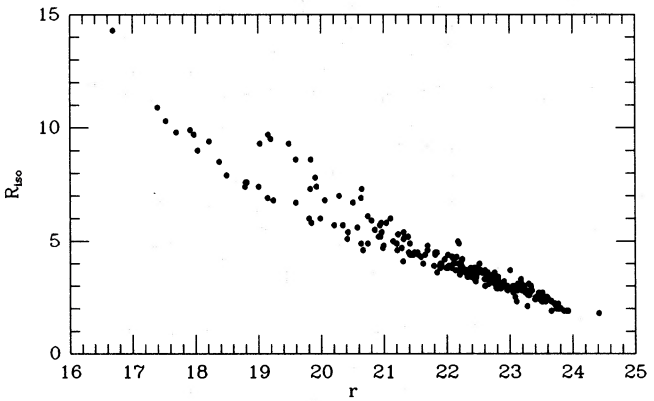

Figure 4. Isophotal radii of the objects in our photometric catalogue versus their r magnitude. For magnitudes brighter than $r \sim 21$, the sequence branches, discriminating extended objects (upper branch) and stars (lower branch).

3.2 Photometric calibration

Automatic photometry is a very easy job for INVENTORY, collecting a wide set of measures in a reasonably short computational time. It is important, however, to get a realistic estimate of the accuracy achieved, since we are dealing with objects at unfavourable signal-to-noise ratios. There are two main combined sources of uncertainty, the first due to statistical scatter of the signal, and the second induced by the transformation to the standard photometric system, through observed reference stars.

Photometric calibration was performed by observing a selected set of standard stars taken from the compilations by Feige (1958) and Landolt (1973), as listed in Table 3. Unfortunately, magnitudes in the Gunn system are not available, and we had to infer them from V and $(B-V)$ data in the Johnson system. Analytical relations linking the two systems can be found, or derived directly, from the list of the Gunn primary standard stars (Thuan & Gunn 1976; Wade *et al.* 1979; Kent 1985). We decided, however, to follow a different procedure, since no reliable transformations are provided in the literature linking the i-band, and no direct evaluation is allowed due to a too coarse set of primary standard stars.

We then used the spectrophotometric catalogue of Vilnius (Strajzhis & Sviderskene 1972), which collects the observed energy distribution (SED) for stars of different spectral types. Direct convolution of the set of spectra with our instrumental

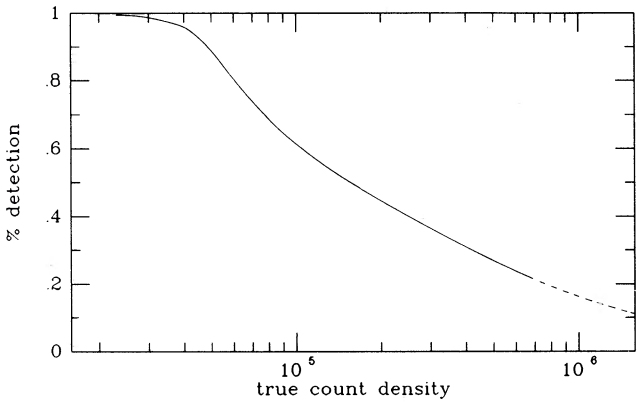

Figure 5. Efficiency (per cent) in the detection algorithm of INVENTORY with varying object density in the frame. Counts are in unit of objects degree^{-2}.

Table 3. Standard stars used for photometric calibration.

Name	B	B-V	g	r	i
FEIGE 11	11.80	-0.26	11.93	12.72	13.02
FEIGE 16	12.45	-0.02	12.42	12.95	13.17
L - 249	12.39	0.65	11.89	11.74	11.70
L - 252	12.36	0.59	11.90	11.81	11.80
L - 284	12.15	1.36	11.16	10.27	9.97
L - 288	11.47	0.60	11.01	10.90	10.88
L - 346	9.87	0.60	9.41	9.30	9.28
L - 351	9.99	0.20	9.81	10.11	10.24

filter responses and with Johnson's ones (Ažusienis & Straižys 1969) provided the required relations of transformation. Magnitude offsets were derived assuming zero colours for a mean A0V star in the Johnson system, while for the Gunn primary standard star BD+17°4708 (Oke & Gunn 1983) we assume $g=r=i=9.5$. The results are shown in Fig. 6.

Using stars with $(B-V)\leq 1.45$, we derived the following set of equations:

$$g=B-0.694(B-V)-0.046 \qquad \sigma=\pm 0.017 \text{ mag}, \qquad (1)$$

$$r=V-0.723(B-V)+0.468 \qquad \sigma=\pm 0.021 \text{ mag}, \qquad (2)$$

$$i=V-1.099(B-V)+0.674 \qquad \sigma=\pm 0.042 \text{ mag}, \qquad (3)$$

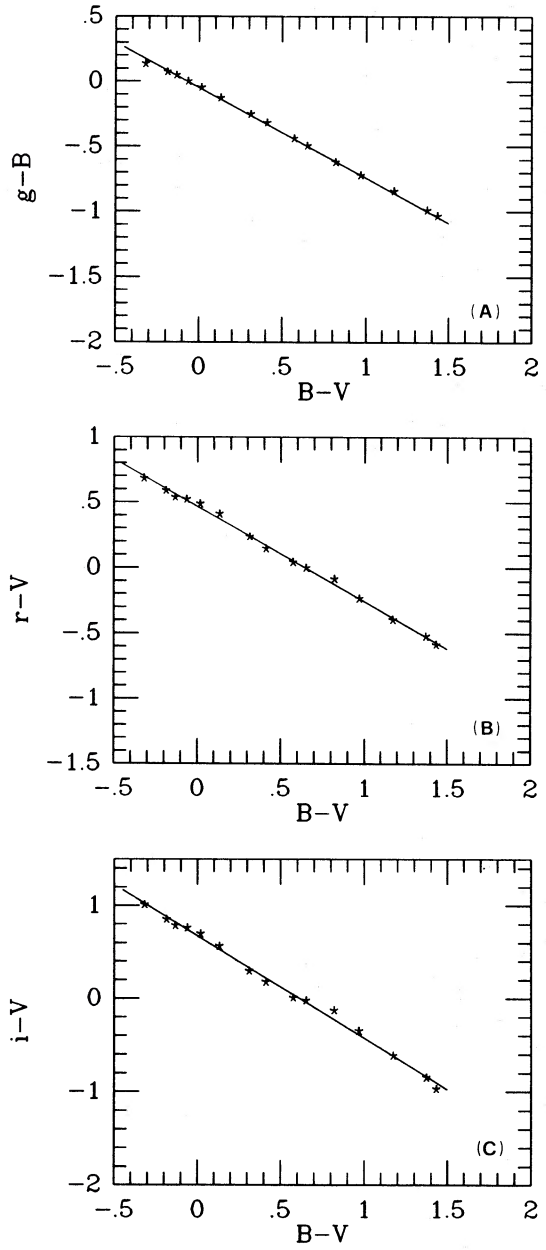

Figure 6. Panels (A)–(C) show the relations of transformation between Gunn *g*, *r*, *i* and Johnson *B* and *V* magnitudes. Asterisks mark stars of different spectral types from the Vilnius catalogue. Adopted regression lines are shown.

where σ is the standard deviation of stars in the Vilnius catalogue around the assumed linear fit.

It is worth stressing that this procedure does not account for the fact that our instrumental system could differ slightly from the canonical Gunn system. As shown in Table 2, some differences could arise for our *i*-band, which is displaced blueward by about 300 Å. However, when compared with the system as defined by Schneider, Gunn & Hoessel (1983), the agreement is nearly perfect. Anyway, comparison of our results with theoretical expectations, as discussed in Sections 5 and 6, has been performed in a quite consistent way, using the same instrumental photometric system. As an independent check for the consistency of our calibration, we derive $(g-r)=-0.548$ for Vega, through the calibration by Hayes & Latham (1975), in good agreement with the colour estimate by Bell & VandenBerg (1987) [i.e. $(g-r)=-0.55$]. Moreover, comparison with Kent's (1985) *g* calibration provides $\delta g=g-g_K=0.14-0.10(B-V)$, while from Thuan & Gunn (1976) we derive $\delta g=g-g_G=0.09-0.06(B-V)$. Residuals from both relations become negligible over the colour range of our observations. Gunn magnitudes, derived for our standard stars by means of the adopted transformation set, are reported in Table 3.

In conclusion, assuming different error sources to be independent, we estimate that the instrumental system matches Gunn magnitudes within 0.06 mag in *g* and *r*, while uncertainty rises to 0.10 mag for the *i*-band. These estimates account for colour equations, for the standard deviation in equations (1)–(3), and for instrumental precision in observing standard stars.

3.3 Photometric accuracy

Photometry of faint objects can be strongly affected by the treatment of the background. This must be evaluated in a portion of the image free from any feature, but close enough to each object to avoid any perverse effect induced by gradients in the sky luminosity or by crowding. Direct inspection of the *r* frame, for instance, reveals that residual low spatial frequencies in the background have an amplitude of the order of 2.5 per cent, while statistical scatter around local mean values is of the order of 0.8 per cent.

In practice, INVENTORY considered a square area of fixed size (we chose 31×31 pixels) centred on each object. Contributions from spurious objects, affecting background by more than 2σ, were removed iteratively, finally retaining the mode of pixel-intensity distribution as fiducial background intensity. Operationally, the mode was estimated as [3 × median − 2 × mean].

As an additional source of error, Poissonian fluctuation in the signal also induces an intrinsic uncertainty δm in the magnitude *m* depending on $10^{0.2}$ mag. Fig. 7 shows the distribution of the magnitude differences of the same objects measured in two *r* frames at 1500 and 1200 s exposure times. The exponential trend is clearly seen, and we can attribute a 1σ envelope such as $\sigma=0.17$ magnitudes at $r=22$. From Fig. 7, we infer the σ_{3000} expected at 3000 s exposure in the co-added final images. Since

$$\sigma^2=\sigma^2_{1500}+\sigma^2_{1200}=2\sigma^2_{3000}+2.5\sigma^2_{3000}, \qquad (4)$$

we derive $\sigma_{3000}=0.08$ mag at $r=22$. Thus we conclude that our photometry is accurate typically within 0.1 mag in the

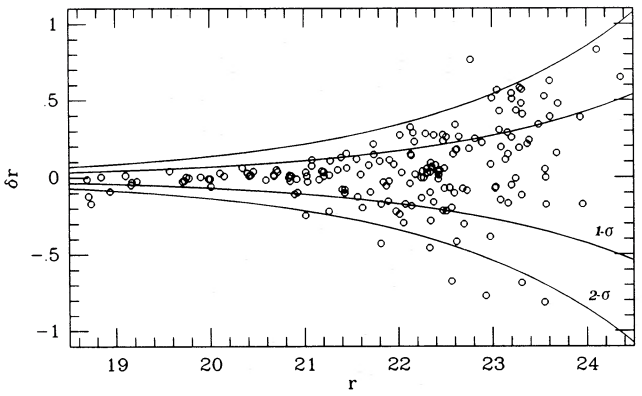

Figure 7. Distribution of the magnitude differences of the same objects measured in two different r frames of comparable exposure times (i.e. 20 and 25 min). Solid lines encompass 1σ and 2σ envelopes. Mean standard deviation is 0.17 mag at $r=22$.

relevant range for the three bands, the uncertainty rising to ± 0.3 mag close to the frame detection limit, i.e. at $g \simeq 25.0$, $r \simeq 23.5$ and $i \simeq 23.5$. Fainter objects in our frames have a S/N ratio of about 30 in g, and 50 in r and i, integrating over a circular aperture of radius two pixels.

4 THE CATALOGUE

Three preliminary catalogues of objects, one for each photometric band, were compiled using only final co-added images. Each list of objects, detected automatically by INVENTORY, was subsequently verified by eye inspection on the frames, and evident defects and spurious features removed. The final list merged all the objects having magnitude in at least one band: the catalogue is reported in Table 4, and collects all relevant photometric quantities for 294 stars and galaxies in the field surveyed. Their finding charts are displayed in Fig. 8.

To assure self-consistency, magnitudes and colours for the objects in the catalogue were derived in two different ways. Integrated magnitudes were obtained at a fixed isophotal level, to avoid arbitrary light loss or undesired sky sampling through fixed-aperture photometry. The cut-off isophote was chosen 0.3 per cent above the mean local background, i.e. at a surface brightness 6.3 mag fainter than the sky luminosity. This corresponds to $g=27.86$, $r=26.97$ and $i=26.03$ mag arcsec^{-2}.

In principle, a further correction would be necessary to the isophotal magnitudes of the galaxies to recover loss of light due to redshift effects. At large distances, the outer regions of the galaxies fade to undetectable values for the surface brightness, and this effect is expected to increase with redshift. As a consequence, the galaxies' apparent total luminosity would be underestimated. Following the procedure outlined in Jarvis & Tyson (1981), our isophotal luminosities would be underestimated. Following the galaxies' total light, and a correction $\Delta m=0.07$ mag would be required.

We did not correct our magnitudes for such an effect owing to the fact that (faint) galaxies in our sample are recognized only in a probabilistic way. Moreover, the derived galaxy-luminosity function is only negligibly affected, and in no cases do we expect consequences on colours.

These were calculated at a fixed aperture, since the same metric area on the object has to be sampled in the different photometric bands. In practice, we derived $(g-r)$ and $(g-i)$ colours for each object over two circular apertures with radii of 2 and 3 pixels, finally retaining those at the larger aperture still compatible with isophotal radius in the r-band. It is worth stressing that consistency in our procedure is assured by the very homogeneous point-spread function in the co-added g, r and i frames.

From the work of Burstein & Heiles (1982), we estimate a colour excess $E_{(B-V)}=0.04$ about the galactic coordinates of the cluster (i.e. $l=63°$ and $b=-38°$). This value has to be considered as very tentative due both to the low resolution in Burstein and Heiles' reddening map, and to the possible local irregularities throughout our field. A lower value for reddening [i.e. $E_{(B-V)}=0.02$] is inferred from Sandage's (1973) absorption-free polar-cap model, while de Vaucouleurs, de Vaucouleurs & Corwin (1976) predict $E_{(B-V)}=0.08$ in this zone. We avoid any correction to the observed magnitudes and colours, just deferring analysis of the reddening effects to Section 6, when discussing overall photometric properties of the cluster-galaxy population.

The quantities listed in Table 4 are in the order: identification number; local x and y coordinates in pixels; isophotal radius (R_{iso}) in pixels in the r-band; the g, r, i magnitudes; the integrated $(g-r)$ and $(g-i)$ colours, derived via the above described procedure; and finally, wherever possible, the estimated probability (P_{gal}) of cluster membership for the objects, as we will discuss in Section 4.1. The centre of our local coordinate system is placed at $\alpha_{1950}=22^h00^m44^s$, $\delta_{1950}=0.4°05'20''$ with an uncertainty beam of ± 1 arcmin due to automatic encoding of the telescope position. We have also added to the catalogue three bright stars (nos 292, 293 and 294) appearing as saturated features on the frames, and for which no accurate magnitudes can be obtained. A rough estimate for them gives $r \sim 15.5$–16.5.

Over the total of 294 objects, 247 were detected in g, 242 in r and 196 in i, 230 have at least one colour, and for 161 we have complete photometry in the three bands.

4.1 Membership and contamination

In attempting a study of cluster-galaxy population, we need to 'extract' it from the rest of the objects in the fore- and background. This operation can be conceived in many different ways, and it does not necessarily require a direct selection of all single galaxies in the cluster. Our goal is therefore to pick up global cluster properties over what we can generically call 'contaminations'.

Contaminations are caused essentially by stars of the Galaxy and by field galaxies along the line-of-sight of the cluster. As a usual approach to the cleaning procedure, one could evidence characteristic trends in morphological and/or photometric indices computed for resolved bright stars and galaxies, then attempting an extrapolation down to the faint magnitudes (e.g. Kron 1980; Koo 1981; Jarvis & Tyson 1981; Koo *et al.* 1986; Tyson 1988).

We see at least two weak points in this approach. (i) The different behaviour of the morphological parameters, marking stars and galaxies, always vanishes at the very faint magnitudes pertinent to distant clusters, and the two populations of objects fatally merge together. (ii) Let us suppose we

Table 4. The catalogue.

No.	x	y	R_{iso}	g	r	i	(g-r)	(g-i)	P_{gal}
1	-60.0	-257.4	1.9		23.93	23.36			
2	-69.5	-256.3	3.2	22.20	22.46		-0.18		
3	23.3	-251.3	2.7	23.97	23.06		1.08		
4	-156.6	-250.3	3.5	23.28	22.66		0.63		
5	-159.9	-246.4	2.8		23.12	22.57			
6	-125.1	-243.3	7.6	19.68	18.80	18.29	0.87	1.31	0.00
7	-158.0	-239.4		23.58					
8	-33.2	-239.4	3.2	23.41	22.91		0.58		
9	25.6	-236.5	2.7		23.26				
10	43.3	-236.4	3.0	23.02	23.08	21.36	0.08	1.62	
11	37.2	-233.3	7.4	19.91	19.01	18.55	0.88	1.29	0.00
12	3.6	-229.9		24.69		22.66		1.95	
13	43.9	-227.7		24.34					
14	5.9	-226.7	2.8		23.23	22.66			
15	119.9	-224.6	2.7	23.08	23.25	21.53	0.31	1.46	
16	-162.6	-217.9	3.2	23.09	22.83		0.38		
17	-109.9	-214.9	8.5	19.32	18.38	17.56	0.95	1.66	0.00
18	7.0	-214.0	3.6	22.82	22.49		0.34		
19	-124.1	-212.9	5.7	21.27	20.35	19.74	0.93	1.47	0.00
20	103.8	-209.1	3.3	23.72	23.18		0.48		
21	-130.9	-205.3		24.28					
22	-126.8	-199.5		23.72					
23	61.1	-199.2	7.3	22.17	20.65	20.52	1.31	1.70	
24	103.0	-197.6		24.14					
25	-128.2	-188.6	2.2		23.77	22.88			
26	38.0	-182.2	3.5	23.95	22.34	21.75	1.53	2.10	
27	45.8	-181.1		24.59					
28	2.2	-180.1	2.0		23.74	22.95			
29	-44.6	-179.9		24.35					
30	-96.0	-178.4	6.9	19.90	19.15	18.66	0.77	1.18	0.00
31	56.8	-174.9		24.35					
32	64.2	-174.0	5.7	20.87	20.21	20.00	0.70	0.94	0.00
33	-117.5	-173.8	2.3		23.57				
34	77.2	-171.4	3.4	23.33	22.33	21.92	1.07	1.45	
35	-27.9	-169.0		24.55					
36	90.9	-162.8	3.0	23.86	23.34		0.73		
37	-41.3	-162.2	3.6	23.31	22.65	22.40	0.79	1.13	
38	-9.5	-160.8	2.5	24.24	23.46	22.54	0.67	1.62	
39	-36.3	-160.4		24.88					
40	-2.1	-160.2		24.28					
41	29.5	-153.6		24.07					
42	54.9	-139.2	3.4	24.43	22.70	21.47	1.67	2.79	
43	96.7	-139.0	3.9	23.02	22.04	21.76	0.96	1.28	
44	-8.4	-138.3	2.8	22.97	22.96	22.68	0.31	0.64	
45	25.2	-134.6	3.6	24.43	22.58		1.52		
46	-39.6	-133.7	2.0	24.47	23.79		0.79		
47	-103.1	-131.9		24.59					
48	-21.9	-131.7	4.8	22.77	21.70	21.02	0.93	1.56	
49	-110.4	-127.3	2.5	23.12	23.09		0.09		
50	55.9	-124.4		24.53					
51	-107.0	-121.8	4.3	22.89	22.09	21.93	0.76	0.89	
52	-95.9	-117.0	2.3		23.66	22.32			
53	-158.4	-116.2	2.8	24.08	23.23		1.00		
54	89.4	-113.2		23.84					
55	-45.3	-112.4	2.0	24.11	23.74	23.04	0.54	1.07	
56	-119.8	-112.2	4.8	21.85	21.00	20.76	0.82	1.14	
57	32.6	-111.1		24.58					
58	-13.6	-110.3	4.4	23.32	21.82	21.32	1.33	1.82	
59	-158.3	-108.1	4.9	20.70	20.75	20.77	0.00	-0.06	
60	14.2	-107.0	5.9	22.12	20.81	20.68	1.23	1.47	
61	-143.4	-106.6	2.6		23.31				
62	25.2	-104.5		24.45					
63	52.3	-103.3		24.64					
64	9.8	-101.6	4.0	23.98	22.23	22.28	1.48	1.56	
65	37.6	-99.9	10.3	17.37	17.53	17.39	-0.20	-0.08	0.00
66	-6.6	-98.0	2.1	24.20	23.28	22.22	0.99	1.84	
67	-130.9	-97.5	3.7	22.25	22.19	22.37	0.11	0.03	
68	-70.9	-95.7	2.3		23.52	22.71			
69	-16.6	-94.8	4.5	22.28	21.40	21.09	0.88	1.31	0.77
70	87.3	-94.2	3.1	22.52	22.76		-0.11		
71	64.8	-91.6	4.7	22.13	20.99	19.83	1.18	2.25	
72	-13.8	-89.7	4.6	22.59	21.22	20.88	1.39	1.75	0.62
73	-137.7	-89.3	3.4	22.48	22.81		-0.04		
74	-145.5	-83.5	4.6	21.89	20.67	19.33	1.33	2.48	
75	-114.3	-82.9	5.3	22.22	21.23	20.85	1.13	1.58	
76	-88.4	-82.8	5.2	21.60	20.92	20.53	0.71	1.05	
77	-25.2	-81.8	7.0	21.17	20.29	19.93	0.94	1.21	1.00
78	-1.5	-76.9	4.0	22.03	21.91	22.11	0.20	0.13	0.73
79	44.1	-75.6	1.9	24.82	23.90	22.78	0.93	1.85	0.38
80	86.4	-74.6	3.3	23.73	22.45	21.27	1.25	2.23	

Table 4 – *continued.*

No.	x	y	R_{iso}	g	r	i	(g-r)	(g-i)	P_{gal}
81	73.6	−74.0	2.5	24.75	23.55	22.55	1.00	1.77	
82	−38.1	−74.0	5.7	21.73	20.94	20.83	0.82	0.93	0.63
83	82.5	−71.8		24.28		23.05		1.34	
84	97.1	−70.9	5.8	21.95	21.04	20.65	0.88	1.24	
85	52.5	−70.7	3.1	24.16	22.67	22.16	1.48	1.90	0.53
86	114.7	−66.6	5.4	21.62	20.43	19.40	1.19	2.16	1.00
87	70.1	−62.3	4.0	23.42	22.19		1.07		0.64
88	−85.6	−61.0	3.5	22.14	22.21	22.41	0.10	−0.03	
89	−38.5	−60.0	2.6		23.29	21.62			0.30
90	101.6	−59.3		23.93					
91	60.4	−58.1		24.38					0.19
92	−99.6	−58.1	3.8	22.37	21.99	22.23	0.44	0.25	
93	5.1	−56.4	2.7		23.32	22.44			0.47
94	−133.9	−54.5	2.8	23.47	23.27		0.35		
95	96.1	−52.7	6.1	22.13	20.75	20.62	1.28	1.52	
96	−108.0	−47.5	3.9	23.16	22.03	22.69	1.07	0.64	
97	−141.3	−45.0	4.2	22.07	21.97	22.34	0.25	0.10	
98	−36.4	−42.4	2.7	24.03	23.31	23.03	0.94	1.31	0.50
99	64.7	−40.0		24.02					0.33
100	19.9	−37.7		24.34					0.21
101	63.5	−34.6	4.5	23.03	21.54	21.63	1.45	1.48	0.80
102	79.8	−33.4	6.0	20.77	19.99	19.68	0.77	1.05	0.00
103	−111.5	−32.9	2.8	24.03	23.35		0.74		
104	104.0	−32.4	3.0	23.67	22.87		1.01		
105	7.9	−30.6	4.4	22.97	21.42	20.84	1.50	2.00	0.78
106	−20.3	−30.5	5.2	21.86	21.39	21.09	0.45	0.94	0.76
107	96.3	−28.0	6.7	20.61	19.60	18.96	1.01	1.66	0.00
108	63.5	−26.6	8.6	21.10	19.60	19.37	1.44	1.77	1.00
109	37.0	−25.9		23.42					0.48
110	−161.9	−25.3	4.5	23.16	21.82	21.25	1.15	1.72	
111	−73.7	−24.6	4.0	22.78	21.92	21.47	0.97	1.37	0.75
112	20.7	−23.9				23.24			0.30
113	−38.7	−22.1	4.4	22.60	21.44	21.05	1.23	1.55	0.78
114	9.5	−20.1	8.6	21.28	19.84	19.32	1.44	1.89	1.00
115	−8.0	−19.0	1.9		23.66	22.91			0.41
116	48.2	−18.9	1.9		23.86	23.07			0.53
117	−105.4	−16.4	9.8	17.49	17.70	17.60	−0.28	−0.31	0.00
118	−28.6	−15.7	4.7	22.33	21.29	21.55	1.01	0.89	0.76
119	59.4	−14.0	4.4	23.10	21.66	21.47	1.41	1.67	0.80
120	86.7	−10.8	6.0	19.74	19.81	19.76	0.01	−0.05	0.00
121	−130.3	−10.6	5.1	22.63	21.32	20.83	1.31	1.84	
122	−90.0	−9.5	2.9	23.45	22.86	23.44	0.83	0.56	0.89
123	105.3	−8.4	4.2	23.88	22.12	22.33	1.50	1.53	
124	45.6	−6.4	5.5	22.15	20.86	20.41	1.27	1.80	0.61
125	−14.1	−3.7	4.0	24.74	22.52		1.62		0.49
126	57.1	−2.5	3.7		22.52	21.77			0.71
127	−24.0	−2.3	6.8	21.45	20.06	19.66	1.29	1.68	1.00
128	91.6	0.0	3.4	23.63	22.64	22.97	0.92	0.45	0.44
129	−56.7	0.2	3.5	24.26	22.77	22.94	1.33	1.16	0.43
130	−127.0	0.3	3.0	23.43	22.79	21.66	0.89	1.84	
131	25.0	2.2	6.9	22.47	20.64	20.31	1.61	1.94	0.69
132	54.0	3.1	9.3		19.49				0.81
133	49.5	4.2	9.4	18.23	18.22	18.13	0.07	0.16	0.00
134	116.9	5.3	3.0	23.26	22.61	22.70	0.92	0.87	
135	15.0	5.5	5.2	22.26	21.34	20.74	0.95	1.34	0.74
136	−17.1	5.7	2.9	23.25	23.00		0.26		0.54
137	21.4	8.3	9.7	20.74	19.16	18.95	1.49	1.82	1.00
138	33.1	9.6	2.7		23.52				0.22
139	42.4	10.3	4.5	23.24	21.85	21.08	1.09	1.89	0.74
140	27.0	11.3	5.0	23.06	22.18	22.50	0.72	0.91	0.64
141	−92.6	11.9				21.92			0.61
142	41.4	13.2	3.8		22.26				0.62
143	−18.0	14.1	3.7	22.95	22.31	22.06	0.81	1.09	0.61
144	−24.9	14.2	3.0		23.19				0.10
145	69.0	14.4	5.0	22.55	21.15	20.64	1.41	1.84	0.55
146	−12.2	14.6	1.8		24.42	22.24			0.30
147	−71.4	15.0	5.1	20.40	20.42	20.05	0.07	0.14	0.00
148	−28.1	15.7	2.9	24.31	22.85	21.30	1.47	2.28	0.72
149	9.8	16.4	4.6	23.89	21.70	21.85	1.73	1.84	0.80
150	17.9	16.4	4.9	25.02	22.20		2.48		0.64
151	109.7	19.0	4.0	23.62	22.11	22.00	1.42	1.62	
152	79.5	19.3	7.9	18.34	18.50	18.44	−0.12	−0.07	0.00
153	−40.7	19.4	3.7	23.74	22.21	21.58	1.56	2.11	0.76
154	−65.1	19.5		24.70					0.12
155	−6.6	19.7	7.8	21.28	19.91	19.47	1.35	1.75	1.00
156	3.9	21.2	2.7		23.46				0.18
157	8.0	22.6	3.9	23.42	21.91	21.72	1.45	1.66	0.74
158	29.6	22.8	4.0	23.32	21.90	22.03	1.31	1.32	0.74
159	120.0	23.8	7.3	20.05	19.83	19.60	0.39	0.57	1.00
160	−54.3	24.5	3.9	23.88	22.24	22.62	1.36	1.22	0.62

Table 4 – *continued.*

No.	x	y	R_{iso}	g	r	i	(g-r)	(g-i)	P_{gal}
161	-6.4	25.8				22.60			0.44
162	87.3	26.0	3.7	23.30	22.54	23.27	0.75	0.27	0.76
163	-160.8	26.1	5.4	22.76	21.32	21.08	1.37	1.76	
164	-10.6	27.4	3.6	23.72	22.40		1.25		0.58
165	2.8	31.1				23.20			0.35
166	112.6	32.0	7.4	19.74	18.79	18.21	0.95	1.50	0.00
167	32.0	35.2		24.60					0.09
168	-41.1	36.6	2.5	24.25	23.41		0.83		0.28
169	72.0	36.7		24.37					0.19
170	-9.6	38.1	2.9	24.25	22.81	22.80	1.52	1.63	0.38
171	-12.8	38.1	2.6		23.31				0.15
172	30.3	38.8	2.9	24.38	22.97	22.36	1.39	2.12	0.50
173	80.1	39.7	3.8	23.47	22.08	22.32	1.33	1.36	0.67
174	35.0	43.6				22.68			0.42
175	91.8	44.5	3.6	23.45	22.32	22.54	1.22	1.14	
176	99.9	44.8	5.8	22.15	20.96	21.28	0.91	0.87	
177	-71.4	45.5	3.9	22.90	21.80	21.03	1.08	1.83	0.76
178	-34.3	45.7	3.4	23.62	22.71	22.34	0.78	1.23	0.51
179	64.2	48.2	2.3		23.51				0.22
180	-41.6	48.6	4.3	24.83	22.16		2.81		0.65
181	86.0	48.8	2.5	25.03	23.46		1.28		
182	-54.1	49.1	4.2	23.72	22.25	22.24	1.32	1.68	0.62
183	-98.8	49.4	2.5	24.62	23.53		1.03		
184	-119.4	50.7		24.62					
185	-43.1	50.9				22.57			0.44
186	-77.8	51.0	3.8	21.85	21.99	21.78	-0.04	0.18	0.70
187	103.5	52.1	9.7	17.95	17.98	17.86	-0.03	0.07	0.00
188	75.6	52.3	4.3	23.06	21.59	21.25	1.36	1.64	0.80
189	-25.9	53.7	2.4		23.61	23.28			0.77
190	9.4	55.3	3.6	23.15	22.34	21.64	0.95	1.53	0.75
191	26.5	56.0	3.2	23.85	22.76	23.11	1.10	0.96	0.59
192	-31.9	57.1	3.8	23.97	22.02	21.33	1.84	2.40	0.73
193	62.1	58.1	3.6	22.98	21.85	21.55	1.17	1.44	0.76
194	-96.0	60.2	2.4	24.41	23.49	23.18	0.88	1.25	
195	-14.1	60.6	2.8	24.36	23.05	23.48	1.18	0.96	0.90
196	12.4	61.5	4.0	23.25	21.63	21.17	1.57	2.00	0.80
197	16.0	61.6		25.28					0.30
198	-52.2	62.5	3.4	23.01	22.39	22.48	0.73	0.70	0.58
199	-20.7	62.9	3.8	24.02	22.43	22.12	1.42	1.79	0.55
200	8.9	64.8	3.8	23.57	22.25	22.57	1.18	1.02	0.62
201	-23.9	65.1	3.4	23.23	22.47		0.78		0.54
202	-26.9	66.2				22.68			0.42
203	-34.7	73.9	3.1		23.19	22.32			0.50
204	-90.0	74.1	2.9	23.62	22.86	23.05	0.86	0.77	
205	-21.1	78.2	5.6	21.78	20.58	20.31	1.17	1.43	0.69
206	-132.0	79.5		24.28					
207	-84.2	80.5	4.4	22.63	22.02	21.70	0.63	1.10	
208	-61.7	80.5	2.9	24.45	22.79	22.53	1.46	1.73	
209	47.6	81.9	9.5	20.64	19.20	18.87	1.38	1.71	1.00
210	23.1	82.5	4.9	22.23	21.21	21.38	1.04	1.04	0.73
211	66.8	83.5	2.4	23.85	23.48		0.46		
212	9.4	84.9	7.6	19.45	18.82	18.53	0.64	0.92	0.00
213	-73.6	87.5		23.99					
214	-68.8	88.0	6.0	22.68	21.11	20.89	1.40	1.68	
215	109.0	89.4	2.8	23.40	23.19		0.20		
216	-39.0	89.8		23.92					0.32
217	-99.4	90.5	3.7	24.08	22.14	22.16	1.75	1.83	
218	-11.4	92.9	3.0	24.08	23.09		0.73		0.33
219	78.5	93.6	2.5		23.59				
220	99.9	94.6		24.81					
221	21.9	95.1	10.9	17.15	17.40	17.36	-0.35	-0.40	0.00
222	48.6	96.6	2.2		23.71				
223	85.6	98.7	4.5	22.70	21.49	21.07	1.19	1.52	
224	40.6	99.2	2.0		23.81				
225	-102.6	104.0	2.0	23.65	23.77		-0.07		
226	-7.8	105.7		23.66					
227	-163.3	107.7	3.7	22.73	22.61		0.21		
228	40.4	108.5	3.0		22.90	22.42			
229	34.0	109.6	2.3		23.11	22.74			
230	119.9	109.8	3.0	23.77	23.05	21.81	0.82	1.91	
231	-49.1	112.5	2.7	23.08	23.29	22.92	0.06	0.34	
232	-161.5	114.2	2.9	24.57	23.05	22.17	1.40	2.24	
233	-23.4	117.8	3.6	23.53	22.76	23.12	0.66	0.15	
234	94.5	118.0	3.3	24.00	22.60	22.83	1.26	1.15	
235	47.9	118.1	2.4		23.40				
236	-5.4	118.5	3.5	23.02	22.33	22.29	0.66	0.75	
237	-140.8	122.4	3.6	23.24	22.56	22.86	0.78	0.65	
238	-114.9	127.6	4.9	21.65	20.64	19.75	1.02	1.84	
239	-76.1	128.1	2.9		23.19	23.02			

Table 4 – *continued.*

No.	x	y	R_{iso}	g	r	i	(g-r)	(g-i)	P_{gal}
240	16.6	128.5	14.3	16.49	16.69	16.73	−0.39	−0.52	0.00
241	−54.3	128.6	3.0	24.02	23.23		0.77		
242	52.3	129.6	3.3	23.86	22.44	22.51	1.49	1.51	
243	9.0	130.9				19.67			
244	95.6	131.2	7.4	21.11	19.93	18.98	1.21	2.17	1.00
245	67.9	133.2	5.4	22.20	20.97	20.75	1.26	1.59	
246	−145.2	135.0	4.4	22.60	21.55	21.30	1.01	1.23	
247	87.0	138.4		23.30		23.04		0.87	
248	57.1	139.6	2.9		23.10	23.08			
249	46.4	140.3		23.78					
250	96.3	144.1	3.7		23.01	22.67			
251	−122.1	145.0		24.08					
252	13.4	145.6		24.88					
253	44.0	146.0	2.9	24.30	22.95	22.61	1.30	1.67	
254	71.6	146.3	2.4	24.15	23.56		0.78		
255	−12.2	147.5	3.8	23.07	22.23		1.05		
256	−106.3	147.6	3.5	23.85	22.74	22.80	1.10	1.05	
257	−49.7	147.7	3.4	23.32	22.81		0.55		
258	−7.7	148.6	3.8	23.39	21.90	21.32	1.44	1.91	
259	68.2	149.8	3.1		23.13	22.31			
260	94.4	150.4	5.2	22.27	20.95	20.35	1.37	1.81	
261	−25.4	151.1	3.0	23.78	23.09		0.74		
262	−39.9	161.8		24.25					
263	−134.3	163.3	3.8	22.83	22.46	22.94	0.47	0.38	
264	113.5	167.6	3.1		23.30				
265	8.7	167.9	4.4	23.23	21.47	21.17	1.61	1.91	
266	53.1	168.4	3.0	24.01	22.96	22.92	0.91	1.05	
267	87.9	168.4		24.57		22.77		1.66	
268	0.4	169.3	6.7	22.16	20.51	20.16	1.51	1.84	
269	14.6	172.1	5.8	21.10	19.85	18.79	1.26	2.19	0.00
270	3.2	173.3	3.8	22.75	22.38		0.28		
271	−154.9	177.0	3.2	22.13	22.91		−0.61		
272	72.7	178.6	9.9	17.80	17.92	17.88	−0.19	−0.20	0.00
273	−144.2	180.2	3.6	23.38	22.30	21.72	1.04	1.59	
274	−106.3	180.4	3.9	22.06	21.89	22.10	0.24	0.06	
275	95.1	181.6	4.9		21.42	22.14			
276	−10.5	183.1		24.40					
277	−84.8	184.3		24.65					
278	−14.7	186.2		24.20					
279	−26.4	188.9	3.3		22.68				
280	29.7	189.2	3.7	23.51	22.36	21.93	1.12	1.58	
281	12.5	190.3	6.8	20.18	19.24	18.67	0.97	1.46	0.00
282	−128.4	191.0	9.3	19.26	19.03	18.80	0.30	0.51	0.00
283	−35.9	191.5	9.0	17.77	18.04	18.04	−0.34	−0.44	0.00
284	−153.0	196.0	3.5	23.28	22.34	22.23	0.97	1.12	
285	−44.8	197.4	2.9	24.78	23.18		1.54		
286	3.1	201.2	3.7	24.00	22.37	22.21	1.43	1.60	
287	−11.1	201.2	4.1	22.13	21.31	20.86	0.86	1.22	
288	−50.4	206.9	3.4	22.80	22.82		0.25		
289	−79.0	207.6	2.8	24.33	23.24	22.56	0.93	1.54	
290	−130.2	208.2	3.5		22.73	21.94			
291	21.0	211.7	2.8	24.34	23.34		1.04		
292	−145.8	−129.1							
293	−90.3	−152.0							
294	84.8	206.8							

are able to reject field stars and discriminate galaxies in the direction of the cluster: we have no hope of confidently deciding which of them belong to the cluster and which ones are casually projected in its direction (unless we had spectra for each one of them, of course!). It is clear, in our opinion, that any ostensibly deterministic criterion to attribute membership might induce a number of perverse biases (see Koo 1988 for a provoking discussion). Therefore, as we have no hope of attempting any firm discrimination of the nature of objects fainter than 21st magnitude solely on the basis of their apparent morphology, we decided to approach the problem in a fully statistical way, following the simple procedure outlined below.

By definition, in a cluster of galaxies we expect an excess of galaxies with respect to the field, that is assumed to be spatially uniform in a first approximation. Let us now suppose that B_x is the characteristic distribution of the field with respect to the generic quantity x (it could be a magnitude, or colour) and Φ_x its equivalent for the cluster. Both B_x and Φ_x refer to the same unit area. Sampling counts over two different zones, that we call 'target' (t) and 'check' (c) zones, we have

$$N_x^{(t)} = \Phi_x + B_x \tag{5}$$

and

$$N_x^{(c)} = \alpha\Phi_x + B_x, \tag{6}$$

where $0 \le \alpha \le 1$ scales the cluster-density distribution 'affecting' the check zone. Hence, the residual-count distribution δN_x is

$$\delta N_x = N_x^{(t)} - N_x^{(c)} = (1-\alpha)\Phi_x. \tag{7}$$

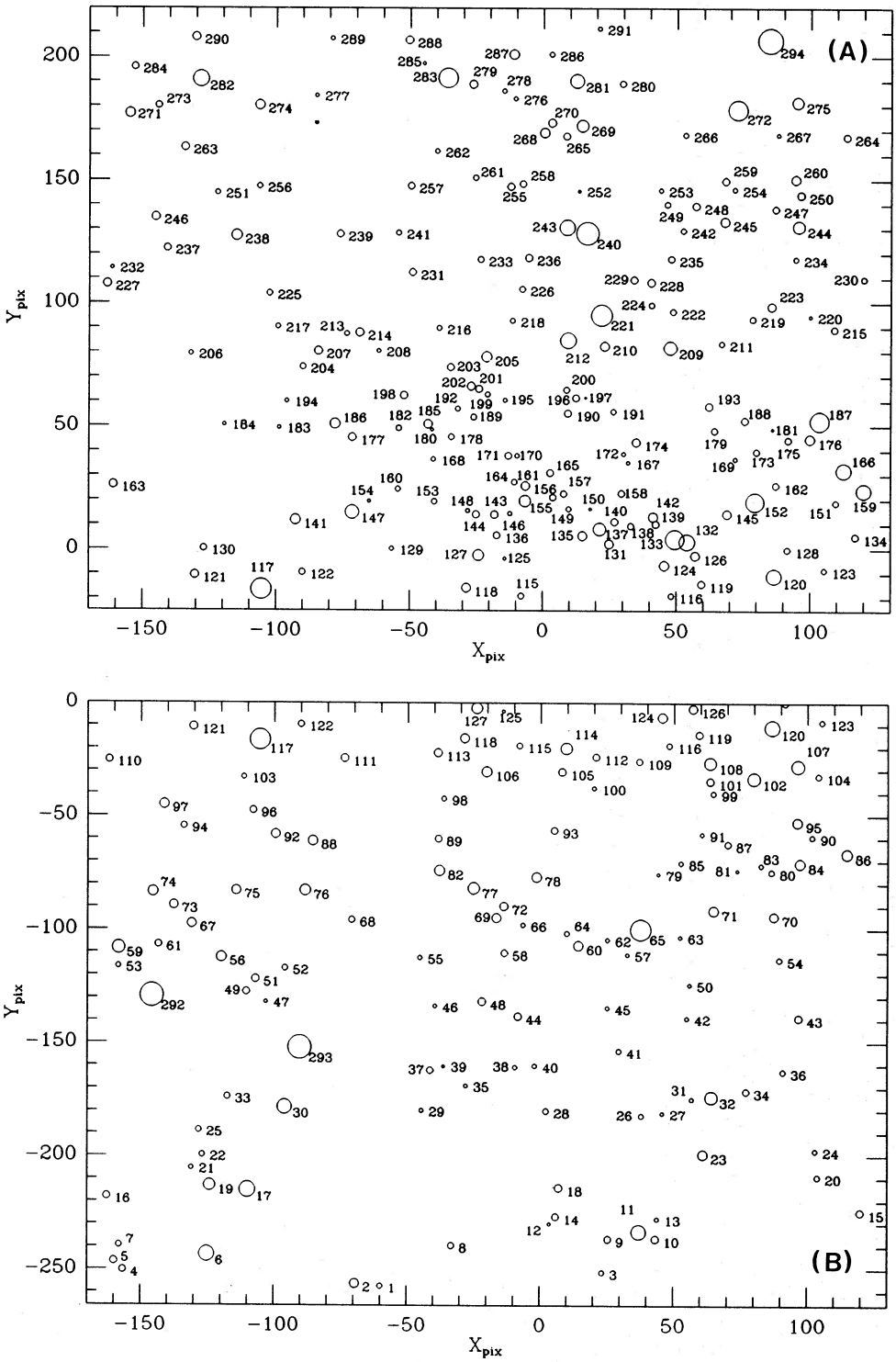

Figure 8. Panels (A) and (B) show identification numbers for the 294 objects in the field of 2158+0351. Spatial units are in pixels: 1 px = 0.675 arcsec. North is up and east to the right.

We see that the unknown cluster-distribution function Φ_x is properly described by δN_x except for a (reducing) scale factor. If we choose the check zone well outside the cluster (i.e. ideally at $\alpha = 0$), δN_x would directly represent Φ_x, since now we are simply subtracting a pure background. It is clear that we have to aim at meeting this case, confining the cluster in the target zone.

We can also write

$$P_x \geq \frac{\delta N}{N^{(t)}} = (1-\alpha)\frac{\Phi_x}{\Phi_x + B_x}, \tag{8}$$

where the ratio $\delta N/N^{(t)}$ gives a lower limit for the probability P_x of an object having a certain value for x to be a member

galaxy of the cluster. The lower limit derives from the fact that in the general case the right-hand side of equation (8) underestimates the ratio [(no. cluster galaxies)/(total no. objects)]. It is worth stressing that no special *a priori* hypotheses for the cluster's composition or extent are needed in the procedure.

In practice, we defined a circular zone at the centre of our local x, y coordinates, with radius 98 pixels. This is our target zone, and corresponds to 0.5 $(50/H_0)$ Mpc at the cluster. Counts were compared with those in the rest of the frame, after scaling them by a factor of 1/3.44, owing to the different sampled area. Cluster-membership probability for each object in the target zone was assumed as $\sup\{P_g, P_r, P_i\}$ with P_g, P_r and P_i determined separately from the luminosity functions in the different bands (see Section 5.2). For the brightest galaxies ($r<20.5$) all over the frame, a direct identification is allowed from Fig. 4. The results are reported in the last column of Table 4, labelled P_{gal}. The bright spiral (no. 159 in our catalogue) is the only clear foreground galaxy in our frames. Its colours seem to suggest a redshift $z \simeq 0.30$.

We estimate that over a total of 104 objects in the innermost region, at least 63 are cluster members, implying 39 per cent background objects (stars + galaxies). This allows us to estimate an expected count density for the background of about 3.9×10^4 objects degree^{-2}. An independent check can be done by directly evaluating the local density at the border of the frame, where the contribution of the cluster galaxies decreases. Here we find a density of 3.8×10^4 objects degree^{-2} in the r-band.

It would be interesting to compare our results with deep galaxy counts over selected blank fields performed by Tyson (1988). This is the deepest count survey available, reaching $B_J = 27$. A link with Tyson's photometric system can be derived combining the relation of transformation from photographic B_J to B given by Kron (1980) with ours relating Gunn and Johnson systems. We obtain

$$B_J = r + 1.45(g-r) + 0.28. \quad (9)$$

Assuming a magnitude limit of $r = 23.5$ and a typical colour $\langle (g-r) \rangle \simeq 1$ for the faintest objects in our field, we have to match Tyson's integrated counts down to $B_J = 25.2$ (assuming negligible differences induced by our different isophotal-magnitude level). At such faint magnitudes, field galaxies are expected to dominate over Galactic stars, and we then assume from Tyson & Jarvis (1979) and Tyson (1988): $\log N = 4.25 + 0.45(B_J - 24)$ for differential counts per unit magnitude in the field at the galactic pole. Accounting for galactic secant extinction law with a coefficient of 0.3 (Jarvis & Tyson 1981), the density expected at our relevant galactic latitude reduces to 3.9×10^4 galaxies degree^{-2}, in good agreement with our estimates. It is worth noting, however, that field-galaxy counts dramatically increase at such faint magnitudes, and small changes in the cut-off magnitude induce appreciable changes in the count density. Anyway, it appears that our cluster has a rather compact structure, and it should be almost completely included in our CCD frames.

5 CLUSTER-GALAXY POPULATION

The photometric catalogue we have assembled provides the database to investigate the general properties of the cluster and its galaxy population. In this section we will focus our attention on the spatial distribution of member galaxies and their overall photometric properties in luminosity and colour.

5.1 Spatial distribution

An objective picture of the cluster is obtained by direct counts of all the detected objects. In Fig. 9 we display a map of smooth surface-count density obtained by filtering the frames with a circular beam of radius 40 pixels. The compact core is clearly evident, with an overdensity of more than a factor of 3 with respect to the background, and no binary or complex substructures seem to appear. It is dominated by a central clump of galaxies where most of the brightest members are located. In particular, it is evident in a trapezium configuration surrounded by a thin plot of faint galaxies (Fig. 9).

The central region is slightly elongated, with an eccentricity $\varepsilon \sim 0.7$ and a position angle $\theta \sim 110°$. Eccentricity decreases to $\varepsilon \sim 0.4$ in the outer regions, with no appreciable twisting in the position angle.

The centre of the cluster can be defined as the mode of the count distribution of the objects projected on both the x- and

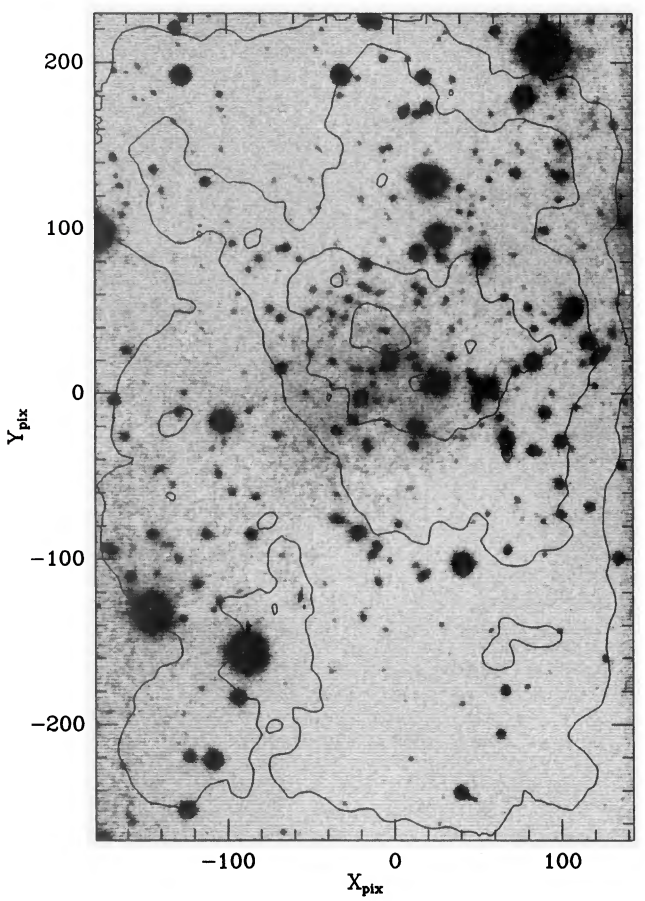

Figure 9. A picture of the cluster in the r-band. It is a co-added image obtained with 50 min total exposure time. Density-contour profiles are superposed, decreasing from 16×10^4 objects degree^{-2}, in the centre of the cluster, to 12, 8 and 4×10^4 objects degree^{-2} in the outer regions of the frame. Spatial coordinates and orientation are as in Fig. 8.

y-axis. It lies at intermediate distance between the density peak visible in Fig. 9 and the trapezium feature, about $(x, y) = (0, 25)$. Centring at this point we obtained the radial profile for surface density by counting objects over concentric rings 20 pixels wide. Counts in the rings overriding the edge of the frame were corrected for incompleteness due to geometry. The result is displayed in Fig. 10. Attempting a fit with a King model, we find a rather compact structure, with a core radius $R_c = 34$ arcsec or 0.25 $(50/H_0)$ Mpc, in perfect agreement with the canonical value proposed, for instance, by Bahcall (1977). The concentration index, as defined by Butcher & Oemler (1984), is $C = 0.44$, consistent with a concentration more enhanced with respect to a uniform-density sphere.

In total, the model predicts about 160 galaxies in the cluster, 69 of which are expected in the target zone, which extends for about $2R_c$. This is consistent with our previous conclusions achieved through the statistical procedure, predicting 63 galaxies. In the Butcher & Oemler (1984) notation, the radius embodying 30 per cent of the total cluster population, R_{30}, is 1.2 arcmin. Assuming a spherical symmetry, we find a mean density of 120 $(H_0/50)^3$ galaxies Mpc^{-3} in the innermost region of the cluster.

5.2 Luminosity function

Knowledge of the luminosity distribution of the galaxies is relevant, since it carries information on the way primeval matter collapsed and lit up. It is also known that dynamical and environmental effects play an important role influencing the morphological genesis and the photometric properties of the galaxies (Schombert 1988; Chincarini 1989). Furthermore, there is no reason to believe that the present-day canonical luminosity function (LF) (Schechter 1976; Abell 1977) also holds in earlier times, since different classes of galaxies have different photometric histories (Bahcall & Tremaine 1988). Therefore, great care should be taken when looking for such possible deviations from the LF which seems to characterize clusters at the present time (Colless 1989).

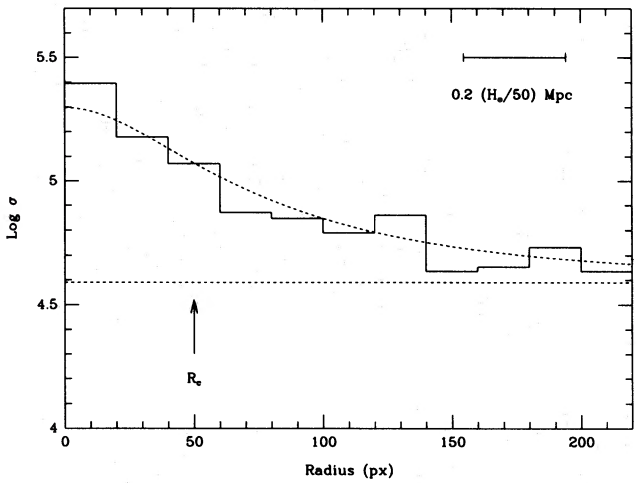

Figure 10. Radial surface-density profile of the cluster. Density σ is in units of counts degree^{-2}. The background level is marked, as well as the fitting King model, and the derived core radius R_c.

The LF for our cluster was calculated in each band, over both the check and target zone, separately. The results are displayed in the three panels of Fig. 11. To ease their comparison, counts in the outermost region have been scaled to the innermost one. An overcount in the target zone due to the cluster is clearly evident at all magnitudes. As we have discussed in Section 4.1, the residual between the two curves in each panel can be supposed to describe the genuine LF in the core of the cluster, removing any background effect. For *g*, *r* and *i* this is shown in Fig. 12.

The most prominent feature one recognizes, comparing Figs 11 and 12, is an abrupt cut-off in the faint tail of the residual core LF, well above the magnitude limit of detection. It is important to note that this does not necessarily imply an absolute lack of galaxies in the centre, but it could result from the lack of completeness in the core due to more severe crowding.

It is also worth mentioning a peculiarity in the LF in Fig. 12, i.e. a lack of galaxies around $r \sim 20.8$. This could be simply a stochastic effect (5–10 galaxies will suffice to compensate for the lack), but nevertheless it is curious to note that the feature can be recognized in all the three bands, and is consistent with the characteristic colours for early-type galaxies, as we will discuss in the next section.

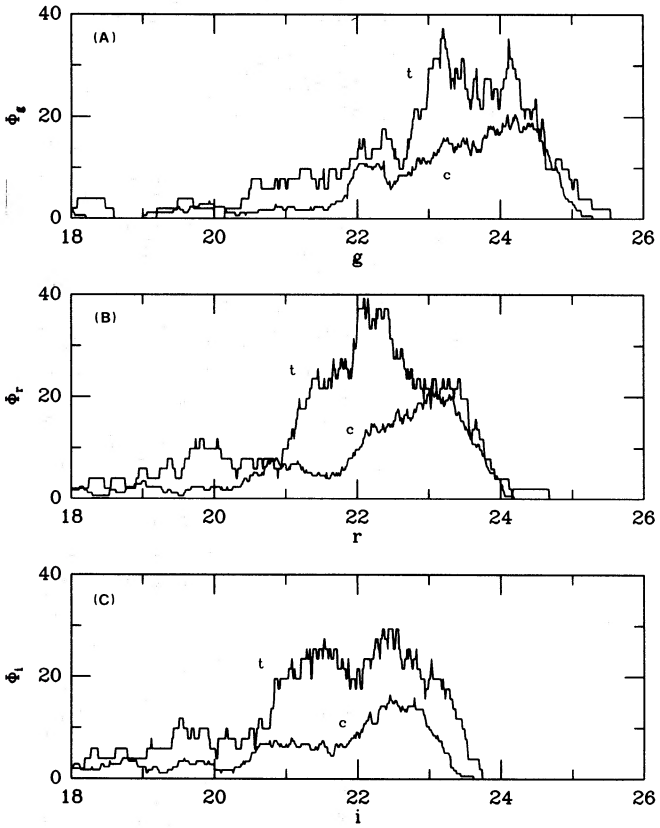

Figure 11. Panels (A)–(C) show differential luminosity functions (in units of objects $\mathrm{magnitude}^{-1}$) in *g*, *r*, and *i*. Two curves are reported in each panel, referring to differential counts in the innermost ('t') and outermost ('c') regions, referred to as the 'target' and 'check' zones, respectively, in the text. Counts from the check zone are reduced by 1/3.44, owing to the different sampled area. Curves are moving averages with a beam of 0.5 mag and a step of 0.01 mag.

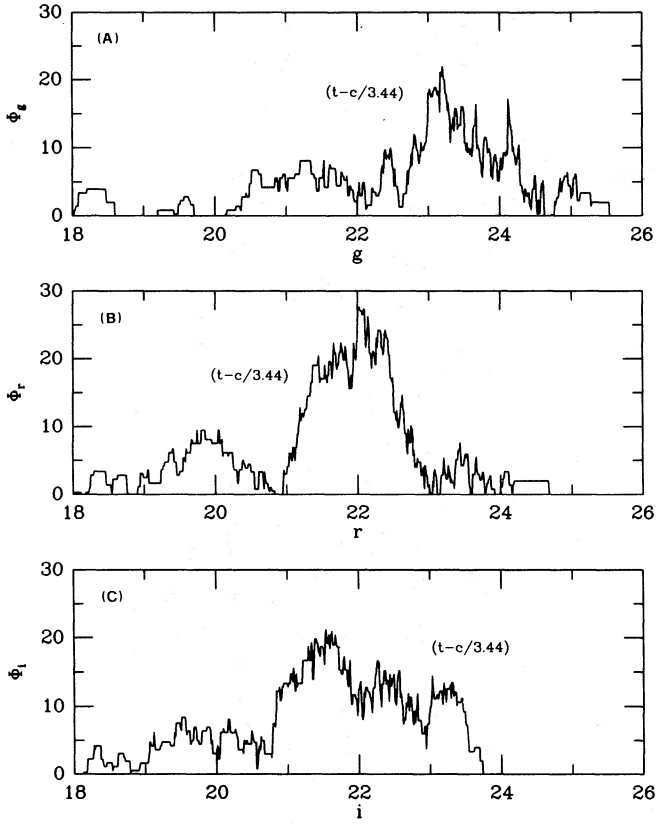

Figure 12. Panels (A)–(C) show the overdensity in the *g*, *r*, *i* core-luminosity function. For each band, the difference between the luminosity function in the target zone and that in the check zone is displayed (reduced by a factor 3.44, owing to the different sampled area). As discussed in the text, this residual can be supposed to describe the intrinsic luminosity function in the core of the cluster. Units are consistent with Fig. 11.

5.3 Colour distribution

A detailed study of the colours is probably our most powerful tool to investigate the properties of the cluster-galaxy population. As we pointed out in Section 3.1, apparent colours of galaxies are a direct consequence of their stellar composition and morphological type. In addition, they change with varying redshift, leading distant galaxies to be even redder than the reddest stars in the galactic field.

In the two panels in Fig. 13 we display the two-colour diagram of all the 161 objects in our catalogue for which photometry in the three bands is available. For the sake of clarity, we compare our observations separately with the loci expected for the stellar sequence, and for galaxies of different morphological types. The stellar strip has been calculated by direct convolution of different SEDs taken from the Vilnius catalogue (Strajzhis & Sviderskene 1972) with our photometric system, according to the absolute calibration discussed in Section 3.2. Colours for different spectral types from F0 to M5 are marked in Fig. 13. It is evident that the stellar locus behaves as a sort of upper envelope for observed points, and only spectral types earlier than K0 seem to match the observations confidently. In panel (B) the colour path expected for spiral and elliptical galaxies with varying redshift is reported. SEDs for the different galaxy types are taken from Pence (1976) for type Sab;

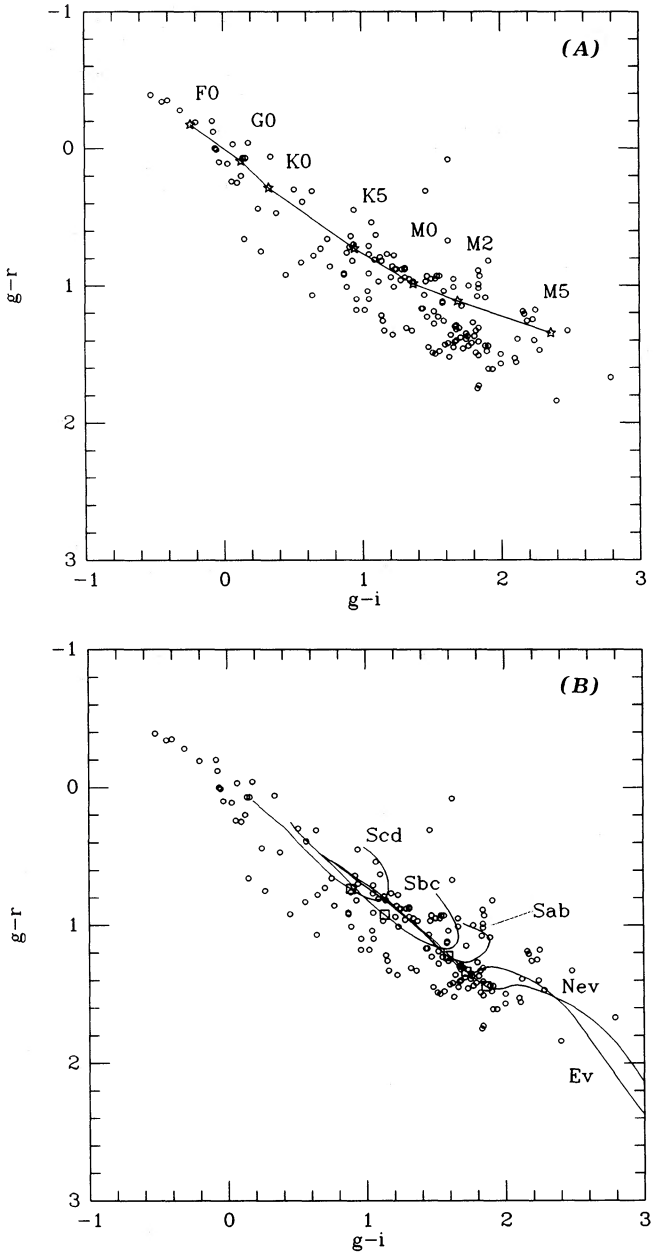

Figure 13. Two-colour diagram for all the 161 objects available in our catalogue. In panel (A), the locus expected for main sequence stars of different spectral types is superposed, while in panel (B) the same is done for galaxies of different morphological types with varying redshift ($0 \le z \le 1$). $(g-i)$ moves redward for increasing redshift, both for spirals and ellipticals, with the spirals forming a hooked feature at large z. For ellipticals, two different loci are displayed, accounting for passive (*Noev*) and active (*Ev*) photometric evolution, as discussed in detail in the text. Small squares mark the values expected at $z = 0.445$.

Coleman, Wu & Weedman (1980) for Sbc and Scd; and Buzzoni (1989) for ellipticals (also accounting for evolution, as we will discuss in detail in Section 6). In Fig. 13, synthetic colours expected at the fiducial redshift of the cluster ($z = 0.445$) are marked with small squares. We are inclined to believe that the red clump of points around $[(g-r), (g-i)] = [1.41 \pm 0.26,\ 1.76 \pm 0.20]$ show a population of elliptical galaxies belonging to the cluster, and seen at an

earlier evolutionary state. (Obviously, since we do not have the possibility to discriminate directly the morphological type, we will talk about *elliptical* and *spiral* galaxies referring only to their expected colours.)

It could be interesting to disaggregate objects according to their magnitude, in order to study how they segregate in colour. The sequence of the eight panels of Fig. 14 summarizes the results. The inner (target) and outermost (check) regions in our frame are compared. The stellar sequence is superposed throughout as a reference. The following conclusions can be drawn from this analysis.

(i) Galactic-field stars dominate the bright foreground ($r<20$) over all the frame, with the only relevant exception of a small group of five elliptical galaxies which are the bright tail of the cluster-galaxy population.

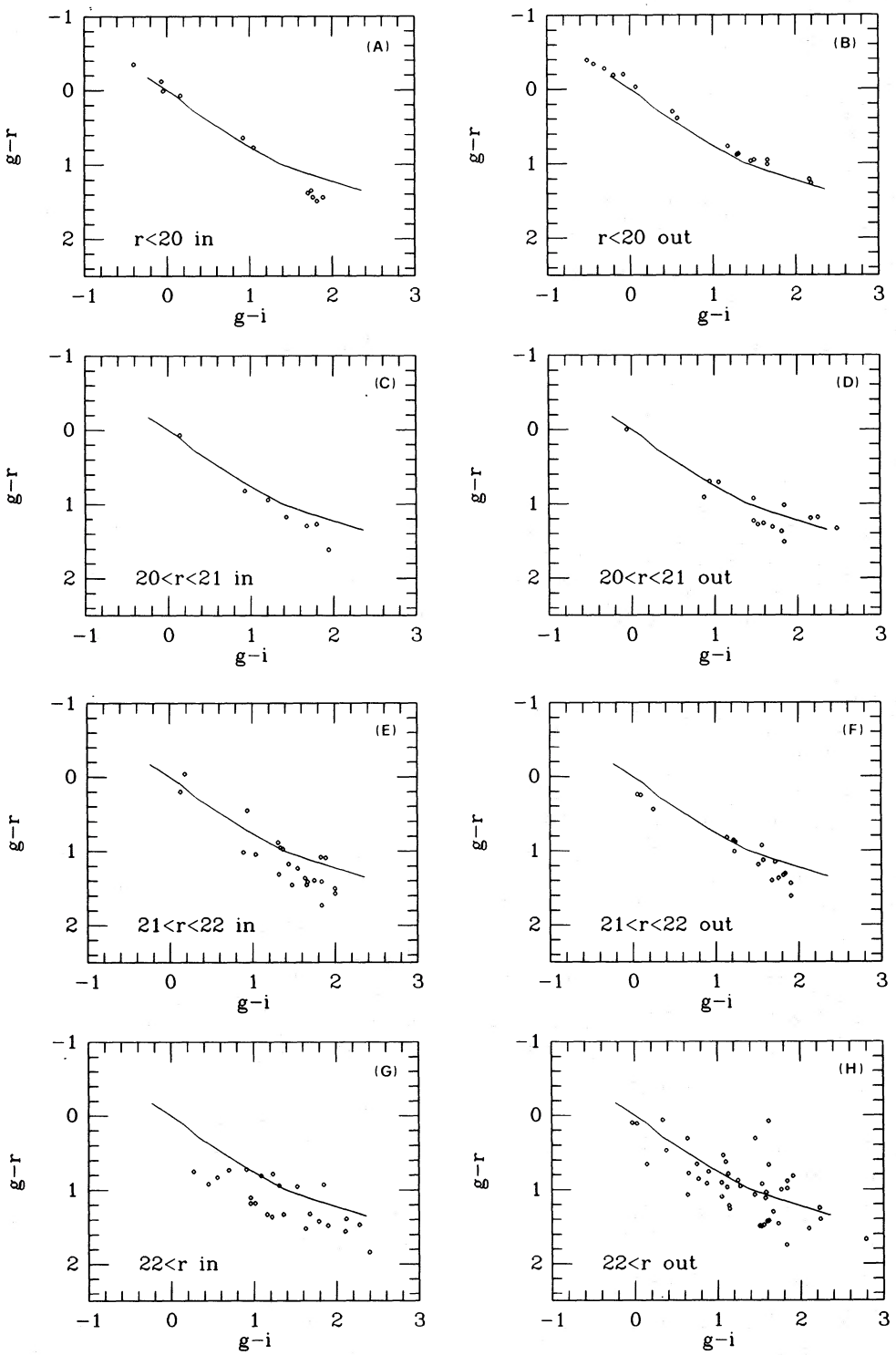

Figure 14. Panels (A)–(H) show two-colour diagrams for objects in different magnitude classes in the *r*-band. The stellar sequence is superposed throughout for reference. See text for discussion.

(ii) All these galaxies reside in the centre (see panel A), and are nos. 108, 114, 137, 155 and 209 in our catalogue. Three of them form the characteristic trapezium configuration well-evident in the picture of the frame (the fourth galaxy in the trapezium is no. 127 with $r=20.06$). It seems clear in this case that a sort of oligarchy of normal ellipticals replaces the role of a single cD, tracing the high-density structure of the cluster.

(iii) Ellipticals dominate in the cluster down to $r\sim 22$, with marginal evidence for an increasing proportion of spirals, probably of types Sab and Sbc, populating the range $1.1<(g-i)<1.6$.

(iv) The ellipticals' leadership becomes less evident among the faintest objects (panels G and H). There is a large spread in the colours and the red clump disappears. The cluster population seems to move blueward, with most of the points below the stellar sequence, especially in the innermost region. This spread is certainly magnified by the increasing photometric error but, nevertheless, it seems too wide to be only an artificial effect, and, in addition, there are no special reasons to expect any systematic bias dimming only r and i magnitudes.

Such a trend is also confirmed in Fig. 15. Here, we show the histogram of the $(g-i)$ distribution for two samples in our catalogue. Panel (A) accounts for all the objects available (165 in total) while in panel (B) we extracted the 69 objects fainter than $r=22$. Again, in panel (A), the double-humped cluster population appears with red ellipticals peaked at $(g-i)=1.68$ taking advantage over the spirals peaked at $(g-i)=1.15$. Galaxy partition strongly changes on going down to faint magnitudes, as shown in panel (B), where the two peaks are nearly equal. This trend is also confirmed, within the statistical scatter, by considering only the innermost region of the cluster and, furthermore, we find that it is mainly induced by the objects in the core of the cluster.

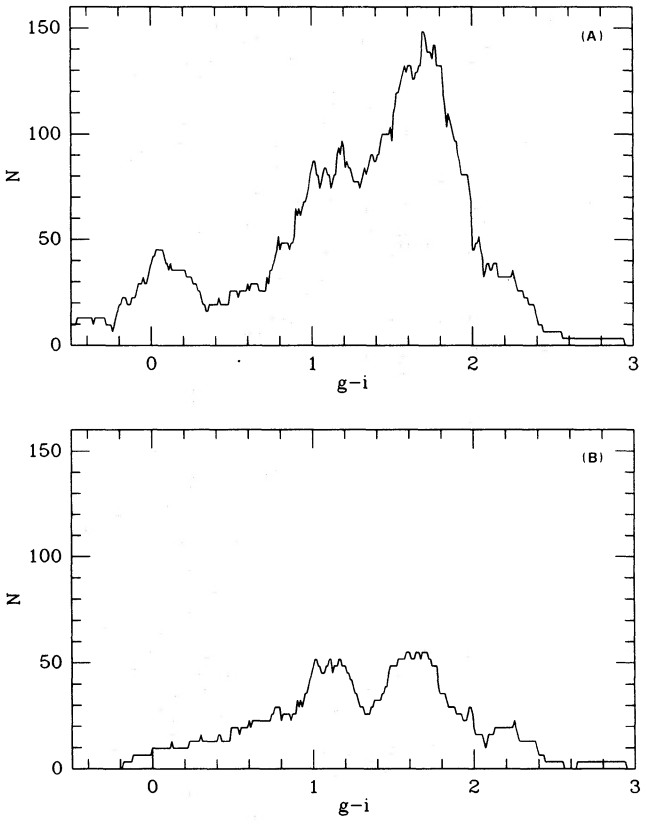

Figure 15. Distribution in the $(g-i)$ colour (objects per magnitude). Panel (A) shows the whole sample available (165 objects on the whole frame), while panel (B) reports only the objects with $r>22$ (65 in total). Curves are moving averages with beam 0.3 mag and step 0.01 mag.

Further information about the cluster-galaxy population can be derived from the colour–magnitude (c–m) diagram collecting the 203 objects in the $(g-r)$ sample. In Fig. 16 one can easily recognize the vertical sequence of the elliptical galaxies, around $(g-r)\sim 1.4$. Despite the photometric uncertainties, a c–m effect might be evident for these galaxies, with bright ellipticals redder than the fainter ones. At the fiducial redshift of 2158+0351, our g- and r-bands are looking at U and B, respectively, in the rest frame, and therefore our observed r versus $(g-r)$ relationship for ellipticals is fully comparable with B versus $(U-B)$ for nearby galaxies. Assuming, as a working hypothesis, that evolution negligibly affects such a relationship, we expect that the slope of the c–m relation will be preserved.

From Visvanathan & Sandage (1977) we calculate $\Delta B/\Delta(U-B)=12$ for early-type galaxies in the Virgo cluster, to be compared in Fig. 16 with $\Delta r/\Delta(g-r)$ in our cluster. We conclude that the expected relationship is consistent with observations, within photometric errors. Clearly, this result does not rule out the fact that an intrinsic colour evolution could have occurred in distant galaxies. Possible effects on the slope of the c–m relationship could hardly be detected within our precision.

Another relevant feature in the c–m diagram concerns a number of blue faint objects, at $(g-R)<0.5$, close to the magnitude limit. Their colours and apparent magnitudes are consistent with main-sequence red dwarfs with spectral types earlier than K0, belonging to the galactic halo. Such evidence confirms equivalent conclusions reached by Tyson

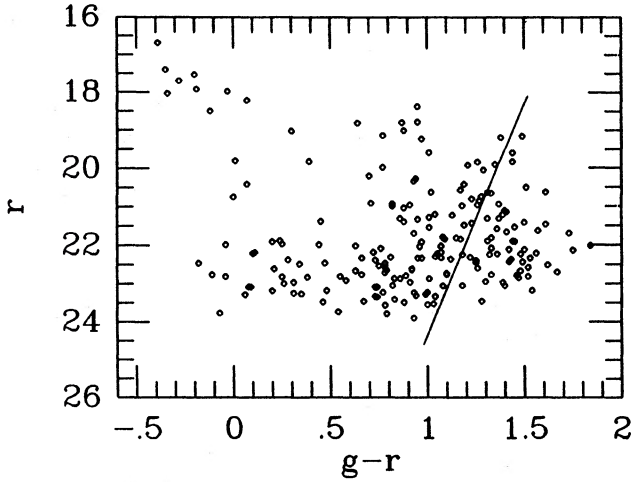

Figure 16. Colour–magnitude diagram, r versus $(g-r)$ for all the 203 objects measured on the whole frame. The relation expected for elliptical galaxies after Visvanathan & Sandage (1977) is also displayed.

(1988). His c–m diagrams also clearly show an abrupt decrease of field stars fainter than $R=22$, in accordance with an assumed envelope of roughly 25 kpc for the galactic halo.

Looking at Fig. 13, however, a (consistent) contribution from field galaxies at very high redshift is not excluded. This would be supported by the fact that most of the bluest faint objects fall below our magnitude limit in *i*. We can therefore infer $(g-i)<0.7$ for them. If so, late-type spiral galaxies at z up to 1 would be the preferred candidates. Conversely, it is unlikely that some high-redshift QSOs hide in such faint objects. Recently, Giallongo & Trevese (1990) have computed evolutionary models for very distant QSOs (z up to 5), following their apparent path in two-colour diagrams. It seems that such objects would populate the region below the stellar strip in the diagram of Fig. 13, so that they can hardly account for the observations.

6 GALAXY EVOLUTION

Changes in the spectral properties of distant galaxies are to be expected as a natural consequence of the time evolution. In our specific case, looking at a cluster at $z=0.445$ would mean that we are looking roughly at $\Delta t=6\times10^9(50/H_0)$ yr back in time ($q_0=0$), i.e. we are spanning one third of the history of the Universe. Evolutionary effects might play an important role in this context, since galaxies are seen in the very early phases of their life. As a consequence, we must account for evolutionary effects when attempting to use clusters as tracers for cosmological topology.

Elliptical galaxies in clusters are recognized as probably the most effective and confident standard candles for cosmological tests. They can reach high intrinsic luminosities and most of their photometric properties can be interpreted in terms of aggregates of coeval stellar populations. Refinements and further complications possibly added to this simplified scenario (we think, for example, of the non-thermal emission in the radio galaxies) do not basically affect the approach (Lilly & Longair 1984).

In addition, we expect that evolution will ease detection of these galaxies which should light up going back in time. This partially recovers the dimming *k*-correction effects. Spirals candidates are not so favourable; they have a more complex history and peculiarities in their star formation lead to less confident interfaces about their photometric properties in the past.

Important improvements occurred in modelling elliptical galaxies through evolutionary stellar-population synthesis (Bruzual 1983; Pickles 1985; Arimoto & Yoshii 1986; Buzzoni 1989). In general, it is found that colour evolution starts to be detectable at $z\sim0.4$ (Koo 1981; Couch *et al.* 1983; MacLaren, Ellis & Couch 1988), while brightening in the absolute magnitudes is evident even at lower redshifts, becoming more and more important at large distances (Tyson 1988).

6.1 Colour and luminosity evolution

Apparent magnitudes and colours of distant galaxies are mainly modulated by two effects: the first induced by the redshift (i.e. the *k*-correction) and the second induced by the intrinsic evolution of galactic SED with time. It is convenient to analyse briefly such different contributions. The influence of the *k*-correction on colours directly derives from a differential effect at the two observing bands. For example, for the apparent $(g-r)_{obs}$ we have

$$(g-r)_{obs}=[g_0+k_g]-[r_0+k_r]=(g-r)_0+\Delta k_{(g-r)}, \tag{10}$$

where $(g-r)_0$ is the colour in the rest frame of the galaxy.

If evolution is accounted for, we can write

$$\begin{aligned}(g-r)_{obs}&=[g_{\Delta t}+(k_g+e_g)]-[r_{\Delta t}+(k_r+e_r)]\\&=(g-r)_{\Delta t}+\Delta k_{ev(g-r)},\end{aligned} \tag{11}$$

where Δt is the look-back time, to be linked with z via the cosmological model. In equation (11) it is convenient to define the *evolutionary* *k*-correction as $k_{ev}=k+e$ with $e_g=g_0-g_{\Delta t}$ and $e_r=r_0-r_{\Delta t}$ for the two bands. Models for elliptical galaxies indicate that evolution is always stronger in magnitude than in colour (Tinsley & Gunn 1976; Buzzoni 1988).

In order to account for evolutionary features in the ellipticals of our cluster we calculated synthetic *k*-corrections and expected apparent $(g-r)$ and $(g-i)$ colours with varying redshift from a grid of models using the code for evolutionary population synthesis by Buzzoni (1989). This is shown in Figs 17 and 18, both for passive (i.e. $e=0$) and active evolution, labelled *Noev* and *Ev*, respectively. At $z=0.445$ one sees that galaxies are brighter by 0.53 mag in *r*, while the apparent $(g-i)$ colour turns blueward by 0.14 mag.

Fig. 18 allows us to calculate the expected path for ellipticals in the two-colour diagram we showed in Fig. 13. As we noted when discussing colour distribution, the observed points for fiducial elliptical galaxies in Fig. 13 statistically clump blueward of what is expected in the absence of photometric evolution. Actually, mean colours for the clump are $(g-r)_{gal}=1.41$ and $(g-i)_{gal}=1.76$, while models predict $(g-r)_{Noev}=1.44$ and $(g-i)_{Noev}=1.86$ in the case of passive *K*-correction and $(g-r)_{ev}=1.34$ and $(g-i)_{ev}=1.72$ once evolution is accounted for. It is worth stressing that observed colours are not corrected for reddening. As we discussed in Section 4, attempting such a correction, we will assume $E_{(g-r)}=1.10\ E_{(B-V)}$ and $E_{(g-i)}=1.73\ E_{(B-V)}$ for colour excesses and $A_g=3.53\ E_{(B-V)}$, $A_r=2.43\ E_{(B-V)}$, $A_i=1.80\ E_{(B-V)}$ for magnitude extinctions. Assuming a conservative range $E_{(B-V)}=0.02-0.08$, we would shift colours to

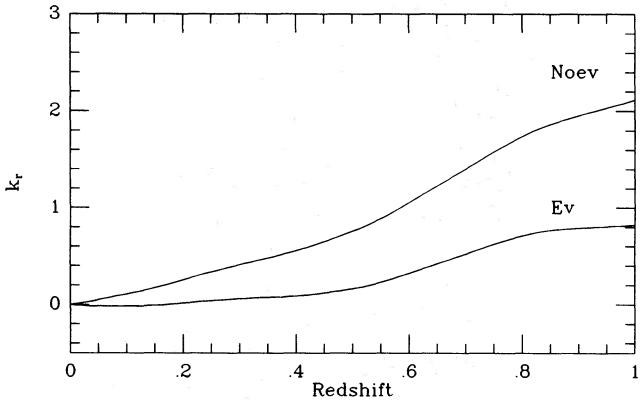

Figure 17. *k*-correction for the *r* passband. The two curves account for passive (*Noev*) and active (*Ev*) photometric evoloution, as discussed in the text.

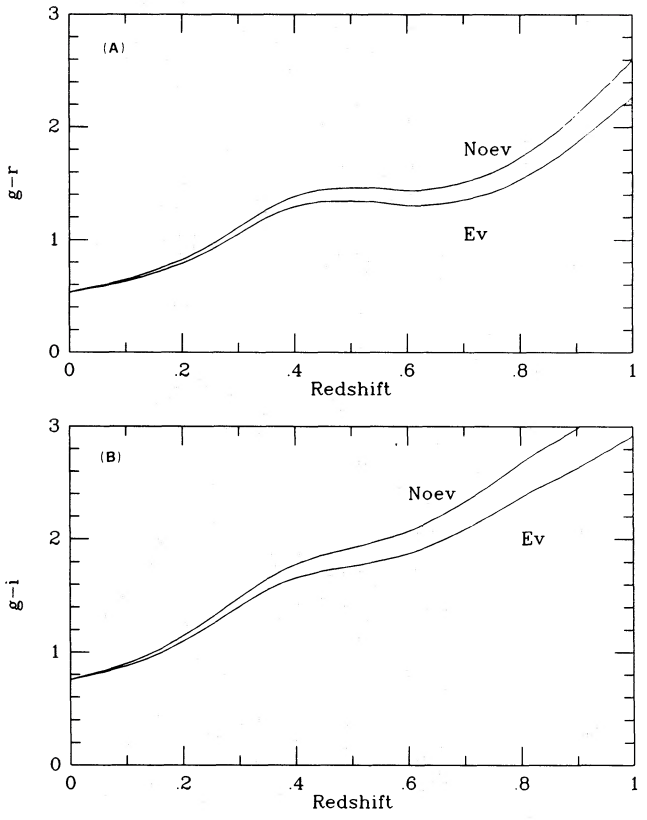

Figure 18. Expected colours $(g-r)$ (panel A) and $(g-i)$ (panel B) for elliptical galaxies, in the case of passive (*Noev*) and active (*Ev*) photometric evolution, as discussed in the text. Synthetic colours are based on the models for evolutionary population synthesis by Buzzoni (1989), and assume an $(H_0, q_0)=(50, 0)$ cosmology.

$(g-r)_{gal}=1.32-1.39$ and $(g-i)_{gal}=1.62-1.73$. As a result, evolutionary models meet the observations even better.

With regard to the detection of intrinsic variations in cluster LFs with cosmic time, a very fine tuning and large cluster statistics would be required, since we are always dealing with the bright part of the distribution, where statistical fluctuations become important.

The absolute r magnitude of a galaxy in the cluster can be derived from

$$M_r = r - k_r - 2.43E_{(B-V)} - 42.567. \quad (12)$$

In equation (12), r refers to the observed magnitude and we account explicitly both for reddening and k-correction. Here, we assume also $(H_0, q_0)=(50, 0)$. From Fig. 17 we calculate that the passive k-correction for ellipticals in the r-band is 0.65 mag, while evolution decreases it to 0.12 mag.

Through equation (12), we derive for the brightest galaxy in the cluster (no. 137 in our catalogue) $M_r=-23.6\pm0.1$ or -24.1 ± 0.1, depending whether or not evolution is accounted for in the k-correction. Note that the inferred absolute luminosity increases in the latter case because the same apparent magnitude would now correspond to a brighter galaxy dimmed by a stronger k-correction. Error bars in our magnitude estimates account for minority effects due to the quoted uncertainty in the reddening. We have assumed $E_{(B-V)}=0.04\pm0.04$ just as a reference value. Since we typically expect $(V-r)=0.1$ for early-type galaxies, previous magnitudes transform into $M_V=-23.5\pm0.1$ or -24.0 ± 0.1, respectively.

In comparison with other authors, Sandage (1972) derived $M_V=-23.25\pm0.32$ for first-ranked normal galaxies in nearby clusters ($z<0.2$), assuming passive k-corrections by Whitford (1971), while Smith & Heckman (1989) found $M_V=-23.06\pm0.08$ studying powerful radio galaxies within $z\sim0.25$. To be consistent, both these values are to be compared with our estimate, obtained through passive k-correction. A further comparison can be attempted with the work by Thuan & Puschell (1989), who report $M_K=-26.3\pm0.3$ for a sample of first-ranked galaxies in nearby Abell clusters. Assuming $(V-K)=3.3$, we infer $M_V=-23.0\pm0.3$.

Therefore, as marginal evidence, it is remarkable to note that our first-ranked galaxy seems to be intrinsically brighter, and, for example, only the fifth member in the cluster could be compared with Sandage's absolute magnitude. Such an enhanced luminosity might also be supported by comparison with the standard LF at $z=0$ (Schechter 1976; Sandage, Binggeli & Tammann 1985; Binggeli, Sandage & Tammann 1988), although statistical fluctuations are certainly important in this regard. A test involving magnitude differences between the six brightest galaxies identified in Section 5.3 is fully consistent with Schechter's (1976) theoretical expectations from the standard local LF (his fig. 4). On the other hand, since all these galaxies are recognized as ellipticals, they possibly evolved in a similar way, thus preventing any differential magnitude effect.

6.2 Blue galaxies and the Butcher–Oemler effect

From emerging evidence, stemming from previous discussions, it appears that a relevant fraction of blue galaxies [i.e. at $(g-i)<1.3$] is present in the cluster population. As we have shown in Fig. 15, this is evident at faint magnitudes, with a two-humped colour distribution, discriminating (fiducial) elliptical and spiral galaxies.

A blueing in the galactic photometric properties would certainly not be a surprising feature, as it is naturally induced by quiescent evolution of the galactic stellar populations. The striking feature, however, is that such a contribution of blue objects might be of genuine intrinsic relevance for the component of spiral galaxies over the total galaxy population in the cluster. This is the well-known Butcher–Oemler (BO) effect, predicting a direct increase of blue-galaxy proportion with increasing redshift.

At present, the reliability of this effect is still highly questionable, and several authors achieved opposite conclusions in this regard (*cf.* Koo 1981; Ellis *et al.* 1985; Koo *et al.* 1988). Actually, following Dressler (1984), it would seem that the BO relationship provides an upper limit to the fraction of blue galaxies in the clusters, and it possibly deals with other (still unknown) overall morphological and dynamical parameters featuring in the evolutionary status of the parent cluster.

In order to give a quantitative estimate of the blue-galaxy component in 2158+0351, we calculated the fraction f_B, as defined by Butcher & Oemler (1984). For the sake of consistency with the authors, we used k-corrections by Pence (1976), but no relevant differences would have been obtained using, for instance, the data of Coleman, Wu &

Weedman (1980) or other current sets. The procedure leads to $f_B = 0.30 \pm 0.13$, where the error bar comes from the formal Poissonian scatter in the numerical ratio of the accounted sample. The BO operational procedure requires the pick up of a sample of galaxies brighter than a fixed absolute magnitude (i.e. $M_V = -20$), and this therefore involves an accurate estimate for the k-correction. Since early-type galaxies are expected to be brighter at high redshift, if we account for this through the evolutionary k-correction, as previously described, we would even increase f_B to 0.36 ± 0.14, since now the elliptical-galaxy sample would be selected at a brighter apparent-magnitude limit.

In computing the colour distribution, we accounted for every object in the target zone on the frames, weighting with its probability to be a cluster-member galaxy, as discussed in Section 4.1. This automatically accounts for a proper background subtraction, allowing us to work with a statistically unbiased sample. Therefore, any overcount of blue galaxies cannot, in our opinion, be due to any systematic background effect.

6.3 Redshift estimate

In previous discussions we showed that theoretical models for early-type galaxies, accounting for evolutionary stellar-population synthesis, are able to confidently match observations of galaxies in distant clusters. It would be interesting now to investigate how effectively broad-band colours can be used to derive the redshift of the clusters photometrically. Such an approach would, in principle, provide a useful tool, especially for extended surveys of distant clusters, where systematic spectroscopy of galaxies would require unattainable observing time. Multicolour photometry would greatly help in these cases, deriving relevant information for the clusters in a much shorter time.

It is worth stressing that our procedure for deriving photometric redshifts relies fully on the whole cluster population of early-type galaxies. This allows us to achieve more confident information with respect to redshift estimates from single galaxies.

Basically, we will try to optimize a merit function defined as the pseudo-Euclidean distance between the clump of elliptical galaxies and the locus of the theoretical models in the $(g-r)$ versus $(g-i)$ diagram. In other words

$$F_{(z)} = \{[(g-r)_z - (g-r)_{\rm gal}]^2 + [(g-i)_z - (g-i)_{\rm gal}]^2\}^{1/2}, \qquad (13)$$

where subscript 'z' refers to synthetic colours with varying redshift, and subscript 'gal' refers to the mean colours of the observed galaxies. The two cases of passive and active evolution were considered for theoretical colours, while observations were corrected for reddening, assuming $E_{(B-V)} = 0.04$. Results are shown in Fig. 19.

A possibly questionable point in this procedure is that a bad evaluation of the reddening correction could lead, in principle, to unreliable results. To evaluate properly such a source of uncertainty, we inferred photometric redshifts through our procedure by changing $E_{(B-V)}$ across a rather wide range, as shown in Fig. 20. One can see that a change $\Delta E_{(B-V)} = \pm 0.05$, around our adopted value, affects z by ± 0.05. Therefore, for a conservative evaluation of the accuracy of our procedure, we derive $z = 0.44 \pm 0.05$ for 2158+0351, once evolution is taken into account, in fair agreement with the spectroscopic redshift given by Gunn, Hoessel & Oke (1986). Conversely, calibrating with passive models, we would estimate $z = 0.38 \pm 0.02$.

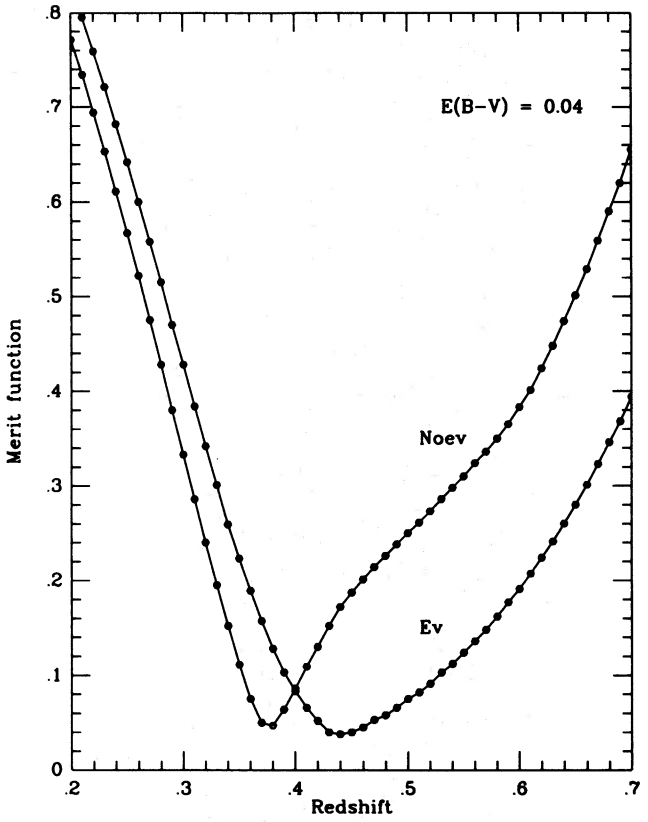

Figure 19. Determination of the photometric redshift for 2158+0351. The merit function $F_{(z)}$, as defined in the text, is minimized at $z = 0.44$ or 0.38 once active (*Ev*) or passive (*Noev*) photometric evolution is accounted for in early-type galaxies. A colour excess $E_{(B-V)} = 0.04$ has been assumed to correct observations for reddening.

As a general conclusion, we point out that as far as distant clusters are concerned (i.e. $z > 0.4$), bad or missing evaluation of photometric corrections for galaxy evolution would strongly bias inferred results, in the sense that galaxies would be recognized as belonging to later morphological types and having systematically lower redshift values.

7 DISCUSSION

As pointed out in Section 1, with the photometric study of the cluster 2158+0351 we intended to outline and test our procedures for reduction of the data, their analysis and comparison with the theoretical expectations. Indeed, a similar approach is in progress for a series of clusters at intermediate and high redshift.

Evolutionary features in the SEDs of the galaxies in 2158+0351 are not expected to be very large in colour, while luminosity is affected by about half a magnitude. Luminosity effects, on the other hand, are somewhat less discriminant: the scatter in a c–m diagram is too large, and a good observational standard has yet to be constructed to clearly single out evolution from a purely observational point of view. However, in this paper we show that a careful com-

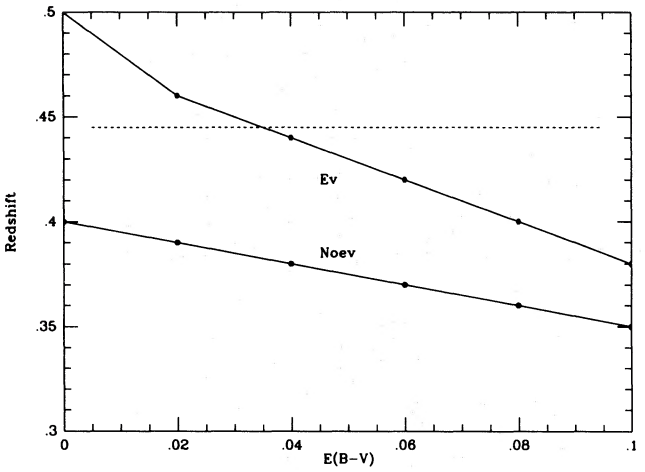

Figure 20. Influence of the reddening correction on the inferred redshift in the adopted procedure. The minimization of the redshift merit function, $F_{(z)}$, is performed with varying colour excess across a wide range. It is, in any case, shown that redshifts inferred from models accounting for galactic photometric evolution better reproduce the fiducial spectroscopic value of Gunn, Hoessel & Oke (1986) (dashed line).

parison of the overall observed photometric properties of the cluster-galaxy population, in a two-colour diagram, with theoretical models is sensitive to evolution.

The importance of taking into account evolutionary effects becomes clear when one attempts to estimate the redshift photometrically. We have shown that in the case of 2158+0351, a discrepancy of about 18 per cent would be introduced by neglecting galaxy-colour changes.

In this cluster, we find clear evidence for a relevant population of blue galaxies. Their fraction, over the total cluster-galaxy population, is about 30 per cent, and this seems to support the claim of Butcher & Oemler (1984) of a marked increase in the blue objects in distant clusters. From the photometric data alone, we are not able to speculate firmly as to the origin of such an anomalous population, which should not be expected in this a high-density cluster (Dressler 1980).

Nevertheless, we are confident that the blue component in the galaxy-colour distribution is real, and not induced by insufficient subtraction of the background or by other biases. As we showed in Fig. 15, there is a net overdensity of objects around $(g-i)\sim 1.2$ in the central region of the cluster, and the effect increases at the faint magnitudes. Actually, a major contribution to the blue-galaxy population comes from objects fainter than $r\sim 21.5$, which means that we are dealing with galaxies fainter than $M_V \geq -21$.

The colours of these galaxies are consistent with normal spirals, and the present analysis does not support any relevant peculiarity as due, for example, to star-burst events involving the early-type galaxy component (O'Connell 1980; MacLaren, Ellis & Couch 1988). In this regard we point out that (i) if stellar formation took place in the ellipticals, we would expect a continuous spread of the colours toward the blue. In no way would this induce the observed biomodality in the colour distribution, unless one invokes quite *ad hoc* conditions; furthermore, (ii) if the blue population consists mainly of mergers or active (elliptical) galaxies, it would be unlikely that this phenomenon involves only the faint tail of the luminosity function, without affecting the brightest members of the cluster.

In conclusion, we are inclined to believe that the unusual population in 2158+0351 fully consists of normal galaxies, and apparent changes in their SEDs are mainly the result of a quiescent evolution of their stellar populations. Of course, this does not rule out the fact that interactions could be present with the cluster environment [Thompson (1988) found a number of BO galaxies to be genuine spirals, often seen in interaction with other cluster members] but this does not seem to affect the overall photometric characteristic of the galaxy population appreciably.

Nevertheless, such an overabundance of spiral galaxies directly relates to a series of problems concerning cluster evolutionary theory. It is clear in fact that the BO effect seems to be in conflict with the evident lack of spirals in the core of the cluster at the present epoch (Dressler 1980). The fate of the spirals seen in 2158+0351 is even more embarrassing when accounting for the fact that the dynamical parameters of the cluster seem to indicate a rather relaxed structure. Concerning this challenging problem, however, we are aware that our statistical approach in sampling cluster-galaxy population could suffer from some limitations, and a spectroscopic study would be certainly more suitable to investigate the cluster dynamics and the specific role played by the spiral-galaxy population.

The bright tail of the cluster LF seems to be dominated by elliptical galaxies, and it shows possible evidence for evolutionary effects. We calculate $M_V=-23.5$ or -24.0 ($H_0=50$) for the first-ranked galaxy, depending on whether or not evolution is accounted for through k-correction. As a peculiarity in the LF of the core of the cluster, we mention an apparent lack of galaxies around $r\sim 20.8$, an effect possibly induced by poor statistics.

Table 5. Summary of the relevant parameters of the cluster.

Coordinates	$\alpha(1950)$	$22^h\ 00^m\ 44^s$
	$\delta(1950)$	$+04^o\ 05'\ 20''$
	l	$+63^o$
	b	-38^o
Redshift	z	0.445
Geometrical Parameters	$P.A.$	110^o
	ϵ_{core}	0.7
Core Radius	R_c	0.6′
		$0.25\ h^{-1}\ Mpc$ (1)
Concentration Parameter	C	0.44
Total Cluster Galaxy Population	N_{tot}	160 gal
Central Density	ρ_{core}	$120\ h^3\ gal/Mpc^3$ (1)
Magnitudes of the First-ranked Galaxy	r	19.16
	M_r	−23.6
B&O Fraction for Blue Galaxies	f_B	0.30 ± 0.13

(1) $h=H_0/(50\ \mathrm{km\ s^{-1}\ Mpc^{-1}})$.

In Table 5, we summarize the relevant distinctive parameters for 2158+0351. The interplay observation–model cannot be completely tested in just one cluster. Indeed, we take the view that the model is tested by knowledge of stellar evolution in systems of stars and galaxies at $z=0$, so that our statement is that, at $z=0.45$, we meet the photometric properties of 2158+0351 as expected.

As the reader will notice, the models do not take into account the possible infall of gas into the single galaxies and its subsequent evolution. In addition, we lack details about galactic photometric properties as a function of the richness class of the parent cluster. This, and other environmental effects, could be significant at such large redshifts (Smith & Heckman 1989).

Our philosophy, however, is that such effects could be singled out after we gain a confident understanding of how clusters and galaxies appear, accounting for the evolution of their normal stellar component. Moreover, we addressed our approach to the cluster-galaxy population as a whole, and this partially overcomes peculiarities due to exotic mechanisms at work in some particular cluster members.

ACKNOWLEDGMENTS

This work is dedicated to the memory of Ioanna Manousoyannaki: she took part in the early phases of this project, and her active contribution and enthusiasm greatly helped in carrying on observations at La Silla and the subsequent data analysis. She should, indeed, have been a co-author. Furthermore, she guided one of us (EM) through the first steps during his thesis work. Ioanna died on 1988 May 9 but her philosophy and approach to science and life, her high respect and love for the human being will always be part of us and our work. This work has been supported by the Italian Ministry for Science and Technology. Thanks are due to Mr S. Cantú for technical help in the editing of the photographic material. Helpful and triggering suggestions, throughout our work, came from Luigi Guzzo. The anonymous referee is also acknowledged for stimulating comments on the early version of this paper.

REFERENCES

Abell, G. O., 1977. *Astrophys. J. Suppl.*, **213,** 327.
Arimoto, N. & Yoshii, Y., 1986. *Astr. Astrophys.*, **164,** 260.
Ažusienis, A. & Straižys, V., 1969. *Soviet Astr.*, **13,** 316.
Bahcall, N. A., 1977. *Ann. Rev. Astr. Astrophys.*, **15,** 505.
Bahcall, N. A., 1988. *Ann. Rev. Astr. Astrophys.*, **26,** 631.
Bahcall, S. R. & Tremaine, S., 1988. *Astrophys. J.*, **326,** L1.
Bell, R. A. & VandenBerg, D. A., 1987. *Astrophys. J. Suppl.*, **63,** 335.
Binggeli, B., Sandage, A. & Tammann, G. A., 1988. *Ann. Rev. Astr. Astrophys.*, **26,** 509.
Bruzual, A. G., 1983. *Astrophys. J.*, **273,** 105.
Burstein, D. & Heiles, C., 1982. *Astr. J.*, **87,** 1165.
Butcher, H. & Oemler, A., 1984. *Astrophys. J.*, **285,** 426.
Buzzoni, A., 1988. In: *Erice Workshop, Towards Understanding Galaxies at Large Redshift,* p. 61, eds Kron, R. G. & Renzini, A., Kluwer, Dordrecht.
Buzzoni, A., 1989. *Astrophys. J. Suppl.*, **71,** 817.
Buzzoni, A., Molinari, E. C., Manousoyannaki, I. & Chincarini, G., 1988. *The Messenger,* **53,** 50.
Chincarini, G., 1989. In: *Lecture Notes in Physics,* Vol. 332, *Morphological Cosmology,* p. 29, eds Flin, P. & Duerbeck, H. W., Springer, Berlin.
Coleman, G. D., Wu, C. & Weedman, D. W., 1980. *Astrophys. J. Suppl.*, **43,** 393.
Colless, M., 1989. *Mon. Not. R. astr. Soc.*, **237,** 799.
Couch, W. J., Ellis, R. S., Godwin, J. & Carter, D., 1983. *Mon. Not. R. astr. Soc.*, **205,** 1287.
Dekker, H. & D'Odorico, S., 1985. ESO Operating manual no. 4.
de Vaucouleurs, G., de Vaucouleurs, A. & Corwin, H. G. Jr, 1976. *Second Reference Catalogue of Bright Galaxies,* The University of Texas Press, Austin.
Dressler, A., 1980. *Astrophys. J.*, **236,** 351.
Dressler, A., 1984. *Ann. Rev. Astr. Astrophys.*, **22,** 185.
Ellingson, E., Yee, H. K. C., Green, R. F. & Kinman, T. D., 1989. *Astr. J.*, **97,** 1539.
Ellis, R. S., Couch, W. J., MacLaren, I. & Koo, D. C., 1985. *Mon. Not. R. astr. Soc.*, **217,** 239.
Feige, J., 1958. *Astrophys. J.*, **128,** 267.
Giallongo, E. & Trevese, D., 1990. *Astrophys. J.*, in press.
Gunn, J. E. & Dressler, A., 1988. In: *Erice Workshop, Towards Understanding Galaxies at Large Redshift,* p. 227, eds Kron, R. G. & Renzini, A., Dordrecht, Kluwer.
Gunn, J. E., Hoessel, J. G. & Oke, J. B., 1986. *Astrophys. J.*, **306,** 30.
Hayes, D. S. & Latham, D. W., 1975. *Astrophys. J.*, **197,** 593.
Iannicola, G., Kalloghlian, A., Nanni, D. & Vignato, A., 1987. *Astr. Astrophys.*, **182,** 189.
Jarvis, J. F. & Tyson, J. A., 1981. *Astr. J.*, **86,** 476.
Kent, S. M., 1985. *Publs astr. Soc. Pacif.*, **97,** 588.
Koo, D. C., 1981. *Astrophys. J.*, **251,** L75.
Koo, D. C., 1988. In: *Erice Workshop, Towards Understanding Galaxies at Large Redshift,* p. 275, eds Kron, R. G. & Renzini, A., Dordrecht, Kluwer.
Koo, D. C., Kron, R. G., Nanni, D., Trevese, D. & Vignato, A., 1986. *Astr. J.*, **91,** 479.
Kron, R. G., 1980. *Astrophys. J. Suppl.*, **43,** 305.
Landolt, A. U., 1973. *Astr. J.*, **78,** 959.
Lilly, S. J. & Longair, M. S., 1984. *Mon. Not. R. astr. Soc.*, **211,** 833.
MacLaren, I., Ellis, R. S. & Couch, W. J., 1988. *Mon. Not. R. astr. Soc.*, **230,** 249.
Molinari, E. C., 1988. *Thesis,* University of Milano.
O'Connell, R. W., 1980. *Astrophys. J.*, **236,** 430.
Oke, J. B. & Gunn, J. E., 1983. *Astrophys. J.*, **266,** 713.
Peebles, P. J. E., 1980. *The Large Scale Structure of the Universe,* Princeton University Press, Princeton.
Pence, W., 1976. *Astrophys. J.*, **203,** 39.
Pickles, A. J., 1985. *Astrophys. J.*, **296,** 340.
Rakos, K. D., Fiala, N. & Schombert, J. M., 1988. *Astrophys. J.*, **328,** 463.
Sandage, A., 1972. *Astrophys. J.*, **178,** 1.
Sandage, A., 1973. *Astrophys. J.*, **183,** 711.
Sandage, A., Binggeli, B. & Tammann, G. A., 1985. *Astr. J.*, **90,** 9.
Scaramella, R., Baiesi-Pillastrini, G., Chincarini, G., Vettolani, G. & Zamorani, G., 1989. *Nature,* **338,** 562.
Schechter, P., 1976. *Astrophys. J.*, **203,** 297.
Schneider, D. P., Gunn, J. E. & Hoessel, J. G., 1983. *Astrophys. J.*, **264,** 337.
Schombert, J. M., 1988. *Astrophys. J.*, **328,** 475.
Smith, E. P. & Heckman, T. M., 1989. *Astrophys. J.*, **341,** 658.
Strajzhis, V. & Sviderskene, Z., 1972. *Bull. Vilnius astr. Obs.*, **35,** 1.
Thompson, L. A., 1988. *Astrophys. J.*, **324,** 112.
Thuan, T. X. & Gunn, J. E., 1976. *Publs astr. Soc. Pacif.*, **88,** 543.
Thuan, T. X. & Puschell, J. J., 1989. *Astrophys. J.*, **346,** 34.
Tinsley, B. M. & Gunn, J. E., 1976. *Astrophys. J.*, **203,** 52.
Tyson, J. A., 1988. *Astr. J.*, **96,** 1.
Tyson, J. A. & Jarvis, J. F., 1979. *Astrophys. J.*, **230,** L153.
Visvanathan, N. & Sandage, A., 1977. *Astrophys. J.*, **216,** 214.
Wade, R. A., Hoessel, J. G., Elias, J. H. & Huchra, J. P., 1979. *Publs astr. Soc. Pacif.*, **71,** 35.
West, R. M. & Kruszewski, A., 1981. *Ir. astr. J.*, **15,** 25.
Whitford, A. E., 1971. *Astrophys. J.*, **169,** 215.